Control of Redundant Pointing Movements Involving the Wrist and Forearm

Garrett R. Dorman
Brigham Young University Neuroscience

Kevin C. Davis
Brigham Young University Neuroscience

Allan W. Peaden
Brigham Young University Mechanical Engineering

Steven K. Charles
Brigham Young University Mechanical Engineering and Neuroscience

Original Publication Citation

G. R. Dorman, K. C. Davis, A. W. Peaden, and S. K. Charles, "Control of redundant pointing movements involving the wrist and forearm," Journal of Neurophysiology (accepted 21 June 2018)

Control of Redundant Pointing Movements Involving the Wrist and Forearm

Garrett R. Dorman[1], Kevin C. Davis[1], Allan W. Peaden[2], Steven K. Charles[1,2]
[1]Neuroscience and [2]Mechanical Engineering
Brigham Young University

Corresponding Author

Steven K. Charles
Mechanical Engineering and Neuroscience
Brigham Young University
435 CTB
Provo, UT 84602
skcharles@byu.edu

Contributions

G. R. Dorman and K. C. Davis contributed to the experimental design, collected data, performed data analysis, and contributed to the writing of the manuscript.
A. W. Peaden contributed to the formulation of hypotheses, performed the initial set of simulations and contributed to the writing of the manuscript.
S. K. Charles was heavily involved in the design of the experiment, the formulation of hypotheses, the data collection, the data analysis, the interpretation, and the writing of the manuscript.

Running head

Redundant Pointing Movements Involving the Wrist and Forearm

Abstract

The musculoskeletal system can move in more ways than are strictly necessary, allowing many tasks to be accomplished with a variety of limb configurations. Why some configurations are preferred has been a focus of motor control research, but most studies have focused on shoulder-elbow or whole-arm movements. This study focuses on movements involving forearm pronation-supination (PS), wrist flexion-extension (FE), and wrist radial-ulnar deviation (RUD), and elucidates how these three degrees of freedom (DOF) combine to perform the common task of pointing, which only requires two DOF. Although pointing is more sensitive to FE and RUD than to PS and could be easily accomplished with FE and RUD alone, subjects tend to involve a small amount of PS. However, *why* we choose this behavior has been unknown and is the focus of this paper. Using a second-order model with lumped parameters, we tested a number of plausible control strategies involving minimization of work, potential energy, torque, and path length. None of these control schemes robustly predicted the observed behavior. However, an alternative control scheme hypothesized to control the DOF that were most important to the task (FE and RUD) and ignore the less important DOF (PS), matched the observed behavior well. In particular, the behavior observed in PS appears to be a mechanical side effect caused by unopposed interaction torques. We conclude that moderately-sized pointing movements involving the wrist and forearm are controlled by ignoring forearm rotation even though this strategy does not robustly minimize work, potential energy, torque, or path length.

New and Noteworthy

Many activities require us to point our hands in a given direction using wrist and forearm rotations. Although there are infinitely many ways to do this, we tend to follow a stereotyped pattern. Why we choose this pattern has been unknown and is the focus of this paper. After testing a variety of hypotheses, we conclude that the pattern results from a simplifying strategy in which we focus on wrist rotations and ignore forearm rotation.

Keywords

Redundancy, pointing, wrist, forearm, Donders

Introduction

Coordinating movements involves the process of mastering redundant degrees of freedom, which allow the body to move in an infinite variety of ways (Bernstein 1967; Latash 2012). Kinematic redundancy enables humans to select preferred limb configurations over others (Burdet et al. 2013). Compared to the many studies of kinematic redundancy involving the shoulder and elbow or the whole arm—for example, see (Scholz et al. 2000; Solnik et al. 2013; Solnik et al. 2014; Yang and Scholz 2005)—relatively few studies have focused specifically on kinematic redundancy in the wrist and forearm even though many everyday manipulation tasks are performed using (mostly or entirely) the wrist and forearm. Here we focus on the task of pointing using the three degrees of freedom (DOF) of the wrist and forearm: wrist flexion-extension (FE), wrist radial-ulnar deviation (RUD), and forearm pronation-supination (PS). Pointing to a target requires only two DOF, so there are infinitely many ways in which the three DOF of the wrist and forearm can be combined to point toward a given target (**Figure 1**).

Campolo et al investigated such pointing movements and found that humans tended to combine these 3 DOF in a repeatable pattern (Campolo et al. 2009; Campolo et al. 2010; Campolo et al. 2011). Following similar investigations involving head-eye movements (Ceylan et al. 2000; Crawford et al. 2003; Ghosh and Wijayasinghe 2012; Glenn and Vilis 1992; Kunin et al. 2007; Radau et al. 1994; Thurtell et al. 2012; Tweed 1997) and unconstrained shoulder-elbow movements (Gielen et al. 1997; Hore et al. 1994; Hore et al. 1992; Liebermann et al. 2006a; Liebermann et al. 2006b; Marotta et al. 2003; Soechting et al. 1995), they expressed this pattern in terms of the rotation vector to determine whether the wrist and forearm followed Donders' Law[1] (Flash et al. 2013). Campolo et al found that the coordinates of the rotation vector did indeed group around a 2-dimensional subspace of the 3-dimensional space of the vector, concluding that redundant wrist and forearm kinematics were constrained to follow Donders' Law. In other words, when humans point using FE, RUD, and PS, they tend to combine these DOF in a stereotyped pattern. In particular, although pointing is more sensitive to FE and RUD than to PS and could be easily accomplished with FE and RUD alone, Campolo et al found that subjects tend to involve a small amount of PS.

However, *why* the neuromuscular system would choose this pattern has been unknown and is the focus of this paper. Applying a variety of common cost functions involving work, potential energy, torque, and path length to a second-order model with lumped parameters, we estimated how subjects would combine these DOF if they minimized one of these cost functions. Interestingly, all cost functions predicted similar behavior in FE and similar behavior in RUD, whereas the predicted behavior in PS varied greatly between cost functions. Therefore, we used the predicted behavior in PS to determine if subjects' pattern minimized a cost function. Surprisingly, none of the common cost functions fit the observed pattern robustly. We turned to an alternative strategy hypothesized to control the DOF that are most important to the task (FE and RUD) and ignore the less important DOF (PS), conjecturing that the observed pattern in PS might be a mechanical side effect of controlling FE and RUD caused by unopposed interaction torques. This hypothesis was found to match the observed behavior closely and robustly. We

---

[1] Donders' Law is an alternative description of how redundant DOF are combined during rotation. Instead of expressing the pattern as a relationship between joint angles, Donders' Law expresses the pattern as a relationship between the coordinates of the total rotation vector (due to rotation in all DOF). Consequently, Donders' Law states that the total rotation vector only occupies a subspace of the total space it could occupy.

conclude that humans tend to control moderately-sized pointing movements (at least up to 22.5°, the largest size tested here) involving the wrist and forearm by ignoring the forearm even though this strategy does not robustly minimize work, potential energy, torque, or path length.

Methods

We 1) performed simulations of pointing movements to determine how subjects would combine FE, RUD, and PS if they minimized common cost functions or ignored PS, 2) ran two experiments of pointing movements to measure how subjects actually combined FE, RUD, and PS, and 3) compared the simulated behavior to the experimentally observed behavior to identify the most plausible control strategy. The methods are presented in this order.

Simulations

We simulated pointing from a center target (at neutral FE, RUD, and PS) to 16 peripheral targets equally distributed on a circle surrounding the center target (**Figure 1**). In general, the peripheral targets were placed 15° from the center target (i.e. the target on the positive x_s-axis could be reached with 15° of wrist extension), and movements were simulated at a comfortable speed (movement duration of 0.5 s). In addition, we simulated movements to farther targets (22.5°) and movements at faster speeds (movement duration of 0.25 s) to test the effect of distance and speed on the predicted movements.

Kinematics

We modeled the kinematics of the pointing task using the coordinates shown in **Figure 1**. The joint coordinate system of the wrist, $x_w y_w z_w$, was centered in the wrist joint, with the x_w-axis pointing volarly, the y_w-axis pointing proximally toward the elbow, and the z_w-axis pointing laterally. PS, FE, and RUD were represented by p, f, and u (defined as positive in pronation, flexion, and ulnar deviation) and occurred about the y_w, $z_w{}'$, and $x_w{}''$ axes, respectively ($z_w{}'$ is the once-rotated z_w-axis, and $x_w{}''$ is the twice-rotated x_w-axis). The orientation of the hand is given by the resulting rotation matrix:

$$R = R_p R_f R_u = \begin{bmatrix} \cos p & 0 & \sin p \\ 0 & 1 & 0 \\ -\sin p & 0 & \cos p \end{bmatrix} \begin{bmatrix} \cos f & -\sin f & 0 \\ \sin f & \cos f & 0 \\ 0 & 0 & 1 \end{bmatrix} \begin{bmatrix} 1 & 0 & 0 \\ 0 & \cos u & -\sin u \\ 0 & \sin u & \cos u \end{bmatrix}$$

$$R = \begin{bmatrix} \cos p \cos f & -\cos p \sin f \cos u + \sin p \sin u & \cos p \sin f \sin u + \sin p \cos u \\ \sin f & \cos f \cos u & -\cos f \sin u \\ -\sin p \cos f & \sin p \sin f \cos u + \cos p \sin u & -\sin p \sin f \sin u + \cos p \cos u \end{bmatrix}$$

The hand points in the negative $y_w{}''$-direction (i.e. in the negative y-direction of the coordinate frame fixed in the hand). Therefore, the direction of the hand, $\vec{r}_h$, is given in the stationary $x_w y_w z_w$-frame by rotating $[0, -1, 0]^T$ by R:

$$\vec{r}_h = R \begin{bmatrix} 0 \\ -1 \\ 0 \end{bmatrix} = \begin{bmatrix} \cos p \sin f \cos u - \sin p \sin u \\ -\cos f \cos u \\ -\sin p \sin f \cos u - \cos p \sin u \end{bmatrix}$$

The location at which subjects' pointed was taken as the tip of $\vec{r}_h$ and indicated by a cursor on a screen in front of the subjects. This screen, defined by coordinates (x_s, y_s), was parallel to the $x_w z_w$-plane, with the x_s-axis pointing in the negative x_w-direction and the y_s-axis pointing in the positive z_w-direction (**Figure 1**). Thus, the relationship between the tip of $\vec{r}_h$, given by (x_w, y_w, z_w), and the cursor, given by (x_s, y_s), was $(x_s, y_s) = (-x_w, z_w)$.[2] Considering the relationship between $\vec{r}_h$ and p, f, and u above results in the following relationship between screen coordinates and joint coordinates:

$$x_s = -\cos p \sin f \cos u + \sin p \sin u \qquad (1)$$

$$y_s = -\sin p \sin f \cos u - \cos p \sin u \qquad (2)$$

Note that although the location to which subjects point, (x_s, y_s), depends on all three joint angles (p, f, and u), it is more sensitive to f and u than to p. This is especially true at the center target ($x_s = y_s = 0$), which requires $f = u = 0$, but there is no constraint on p at the center target (changing p while $f = u = 0$ simply rotates the cursor in place). That said, p does affect (x_s, y_s) at all other locations. Furthermore, its effect on (x_s, y_s) increases with distance from the center target and is therefore greatest at the peripheral targets.

Dynamics

To simulate the dynamics of these pointing movements, we used a joint-level impedance model of wrist and forearm rotations (Peaden and Charles 2014) because it allowed us to test a large variety of control strategies. Joint-level impedance models of wrist/forearm dynamics have been able to explain other movement observations, including path curvature and movement smoothness (Charles and Hogan 2012; Salmond et al. 2017). This model includes the full joint stiffness, damping, and inertia in each DOF (including all coupling terms), gravitational effects, and joint torque. Note that although this joint-level model does not include the muscle level explicitly, it includes musculoskeletal mechanics implicitly: joint stiffness and damping represent the force-length and force-velocity effects of muscle, felt at the joint level. Joint stiffness was measured directly in a similar group of subjects and condensed to its first-order effects (Drake and Charles 2014; Formica et al. 2012; Pando et al. 2014; Seegmiller et al. 2016), and joint damping was estimated from a variety of prior studies (for details, see (Peaden and Charles 2014)). More importantly, we repeated all simulations with a large range of parameter values to determine the effect of under- or overestimating model parameters and other effects, including muscle contraction (see Sensitivity Analysis below).

More specifically, we modeled the dynamics of wrist and forearm rotations as:

$$\vec{M} = I\ddot{\vec{q}} + D\dot{\vec{q}} + K\vec{q} + \vec{G}$$

where $\vec{q} = [p, f, u]^T$ is the angular displacement in the three DOF, with p, f, and u representing PS, FE, and RUD (positive in pronation, flexion, and ulnar deviation), respectively. $\vec{M} = \left[M_p, M_f, M_u\right]^T$ is the torque in each DOF due to active muscle contraction; I, D, and K represent

---

[2] This relationship amounts to a parallel projection of $\vec{r}_h$ onto the $x_s y_s$-plane. For the relatively small movements in this paper, this is similar to a point projection (for movements of 15°, the mean and maximum difference between parallel and point projections are on the order of 1% and 3%, respectively).

the inertia, damping, and stiffness matrices, respectively; and $\vec{G}$ is the torque due to gravity. More specifically,

$$\begin{bmatrix} M_p \\ M_f \\ M_u \end{bmatrix} = \begin{bmatrix} I_{Hy} + I_{Fy} & 0 & 0 \\ 0 & I_{Hz} & 0 \\ 0 & 0 & I_{Hx} \end{bmatrix} \begin{bmatrix} \ddot{p} \\ \ddot{f} \\ \ddot{u} \end{bmatrix} + \begin{bmatrix} D_{pp} & D_{pf} & D_{pu} \\ D_{fp} & D_{ff} & D_{fu} \\ D_{up} & D_{uf} & D_{uu} \end{bmatrix} \begin{bmatrix} \dot{p} \\ \dot{f} \\ \dot{u} \end{bmatrix} + \begin{bmatrix} K_{pp} & K_{pf} & K_{pu} \\ K_{fp} & K_{ff} & K_{fu} \\ K_{up} & K_{uf} & K_{uu} \end{bmatrix} \begin{bmatrix} p \\ f \\ u \end{bmatrix} - glm \begin{bmatrix} f \\ p \\ 1 \end{bmatrix}$$

where I_{Hx}, I_{Hy}, and I_{Hz} represent the inertia of the hand about the body-fixed x, y, and z axes of the hand centered at the wrist joint, respectively (**Figure 1**); I_{Fy} represents the inertia of the forearm about its long axis through its center of mass; and g, l, and m represent the gravitational acceleration, distance from the wrist joint center to the center of mass of the hand, and mass of the hand, respectively. All model parameters were taken from an experiment (Peaden and Charles 2014) involving 5 male and 5 female young, healthy subjects, similar to the present study. More specifically, we averaged the parameters values for male and female subjects used in that study (see Table 2 of (Peaden and Charles 2014)) to obtain a single set of model parameters.

Hypotheses

The model above is under-constrained: for each movement, there are two known variables (x_s, y_s) and three unknown variables (p, f, u), allowing infinitely many solutions. To investigate plausible control strategies, we simulated what (p, f, u) would be if subjects minimized the following hypothesized cost functions: the amount of mechanical work required to execute the pointing movement, the change in potential energy during the movement, the amount of torque required to execute the movement, the amount of torque required to maintain the final pointing posture, and the path length.[3] In addition, we tested a hypothesized simplifying strategy: the pointing movement is planned using only FE and RUD, and any movement in PS results as a secondary effect because the forearm is mechanically coupled to the wrist. Each of these hypotheses is described below.

Mechanical Work: The idea that the body attempts to conserve energy in movement is long standing and has been shown to be accurate in some cases (Alexander 1997). The cost associated with energy conservation used here was mechanical work, defined as

$$C_{MW} = \int_0^{p_f} M_p dp + \int_0^{f_f} M_f df + \int_0^{u_f} M_u du$$

where p_f, f_f, and u_f were the final joint angles (i.e. at the target). Energy expenses resulting from non-mechanical aspects of the system (e.g. chemical processes) were not considered. This hypothesis is therefore akin to choosing the path of least mechanical resistance (impedance).

We used optimization software (the *fmincon* function by Matlab) to find the movement that pointed to the target and minimized the mechanical work. More specifically, the optimization software minimized C_{MW} subject to the non-linear equality given in Equations 1 and 2. Each

[3] The custom-written code used to perform the simulations can be found at https://github.com/BYUneuromechanics/Dorman_JNeurophys_2018.git

simulated movement started at the center target ($p = f = u = 0$) and followed a standard trajectory shape (a minimum-jerk trajectory (Flash and Hogan 1985)) for each joint angle[4] until terminating at a set of joint angles chosen by the optimizer. The movement duration was set to 0.5 seconds, and the applied forces necessary to execute the movement were calculated in intervals of 1ms. The optimization was constrained to keep joint angles within reasonable limits. Movement in FE and RUD was constrained to ±30°, which was greater than the maximum distance from center to peripheral targets (22.5°). Movement in PS was constrained to ±80° to allow peripheral targets to be reached with a large variety of FE-RUD combinations and still remain within the joint limit in PS.

Movement Torque: The neuromuscular system may also attempt to find the movements which minimize joint torque. This differs from minimizing work in that the displacements produced by the applied torques have no direct effect on the cost, making longer joint paths potentially more favorable if they provide less net resistance. The movement-torque cost function was defined as the integral of the magnitude of the torque vector over the duration of the movement:

$$C_{ME} = \int_0^{t_f} |\vec{M}|\, dt$$

where $\vec{M} = M_p\hat{y} + M_f\hat{z}' + M_u\hat{x}''$ and $\hat{y}$, $\hat{z}'$, and $\hat{x}''$ are unit vectors along the y, z', and x'' axes, respectively. Expressing $\vec{M}$ in the xyz-frame as $\vec{M} = M_p\hat{y} + M_f R_p\hat{z} + M_u R_p R_f\hat{x}$ yields

$$\vec{M} = \begin{bmatrix} M_f \sin p + M_u \cos p \cos f \\ M_p + M_u \sin f \\ M_f \cos p - M_u \sin p \cos f \end{bmatrix}$$

Taking the magnitude of $\vec{M}$ and simplifying yields

$$|\vec{M}| = \sqrt{M_p^2 + M_f^2 + M_u^2 + 2M_pM_u \sin f}$$

To minimize this cost function, we used the same optimization software and constraints described above for minimizing work.

Postural Torque: Instead of minimizing torque all along a movement, subjects may have minimized the torque required to hold the final posture (pointing at the target):

$$C_{PEff} = |\vec{M}_f|$$

where subscript f refers to the final posture. Since velocity and acceleration are zero at the final posture, this cost function depended only on the final configuration of the wrist and forearm (p_f, f_f, u_f):

[4] For simplicity, we simulated the minimum-jerk trajectory in joint space instead of task space, but for the size of movements studied here, the resulting trajectory is nearly identical to a minimum-jerk trajectory in screen space as well.

$$\vec{M}_f = K \begin{bmatrix} p_f \\ f_f \\ u_f \end{bmatrix} + glm \begin{bmatrix} -\cos p_f \sin f_f \cos u_f + \sin p_f \sin u_f \\ -\sin p_f \cos f_f \cos u_f \\ \sin p_f \sin f_f \sin u_f - \cos p_f \cos u_f \end{bmatrix}$$

where K is the 3-by-3 stiffness matrix of the wrist and forearm and g, l, and m represent the gravitational acceleration, the distance from the wrist joint center to the center of mass of the hand, and the mass of the hand, respectively (see Supplementary Material of (Peaden and Charles 2014) for derivation). For each target (x_s, y_s), we chose values of p_f between -90° and 90°, computed the associated values of f_f and u_f (i.e. values that satisfied Equations 1 and 2), calculated the cost function C_{PEff}, and found the final wrist and forearm configuration (p_f, f_f, u_f) that minimized that cost function.

Potential Energy: Because the dynamics of wrist and forearm movements are dominated by gravity and stiffness effects (Charles and Hogan 2011; Peaden and Charles 2014), subjects may have minimized the change in potential energy required to make the pointing movement, which is:

$$C_{PEn} = \frac{1}{2} \begin{bmatrix} p_f \\ f_f \\ u_f \end{bmatrix}^T K \begin{bmatrix} p_f \\ f_f \\ u_f \end{bmatrix} - glm\left(\sin p_f \sin f_f \cos u_f + \cos p_f \sin u_f\right)$$

(see Supplementary Material of (Peaden and Charles 2014) for derivation). We found the wrist and forearm configuration (p_f, f_f, u_f) that minimized C_{PEn} using the same methods described above for the postural torque cost function.

Path Length: Subjects may have chosen movements which minimized the total path length. For rotations, the shortest path is a geodesic, which results from rotating from the initial to the final orientation about a single axis. The amount of rotation, ψ, about this axis can be derived from the rotation matrix (Craig 2005):

$$\psi = \operatorname{acos}\left[\frac{1}{2}(R_{11} + R_{22} + R_{33} - 1)\right]$$

where R_{ij} is the element in row i and column j of R. Using the equation for R above, it follows that:

$$\psi = \operatorname{acos}\left[\frac{1}{2}\left(\cos p_f \cos f_f + + \cos p_f \cos u_f + \cos f_f \cos u_f - \sin p_f \sin f_f \sin u_f - 1\right)\right]$$

The angle ψ can be negative (meaning rotation about an oppositely directed vector), so we defined the cost function as the absolute value of ψ:

$$C_{PL} = |\psi|$$

We found the wrist and forearm configuration that minimized C_{PL} using the same methods described above for the postural torque and potential energy cost functions.

Simplifying Strategy: As explained above, pointing is more sensitive to FE and RUD than to PS. Therefore, one potential control strategy may be to simply ignore PS and plan pointing movements with FE and RUD alone. Because PS is mechanically coupled to FE and RUD through stiffness, damping, and inertia (Peaden and Charles 2014), movement in FE and RUD creates interaction torques on PS which, unless opposed, will result in secondary movement in PS.

To test this hypothesis, we ignored PS during the planning stage and computed the effect on PS during the execution stage (**Figure 2**). With only 2 available DOF, the planning stage reduces to a fully constrained problem, so we determined the FE and RUD angles and torques necessary to reach each peripheral target using a 2-DOF model of the wrist, and then executed the movement by forward simulation using the full 3-DOF model of the wrist and forearm (with zero input torque in PS). Mechanical coupling between the DOF caused a "kickback" in PS, which was determined at each target.

Because the movement in PS was not taken into account in the planning stage, the actual final pointing direction was slightly different from the planned direction. However, the error in pointing direction was small (mean error = 1.2°, maximum error = 2.7°) and in practice could be ignored (the targets had a radius of 1.5°) or corrected toward the end of the movement using visual feedback.

Sensitivity Analysis

To determine the robustness of the behavior predicted by each hypothesis, we performed a sensitivity analysis in which we systematically altered the parameters of the model within physiologically plausible ranges and observed the effect on the predicted behavior. We re-ran the simulation for each hypothesis under the following scenarios.

First, we may have under- or overestimated the stiffness parameters. In particular, the stiffness parameters taken from (Peaden and Charles 2014) represent passive joint stiffness (in the absence of contraction), but muscle stiffness is known to increase with contraction (Gomi and Osu 1998; Perreault et al. 2004). Prior studies (Halaki et al. 2006; Milner and Cloutier 1993) have shown that contracting wrist flexor muscles at 15% of maximum voluntary contraction (MVC) yielded measurements of stiffness in FE that were 2-13 times higher than those measured on the relaxed wrist (Drake and Charles 2014; Formica et al. 2012; Pando et al. 2014). The vast majority of wrist muscle activity seen during activities of daily living, which includes movements similar to the movements in our experiment, is below 15% MVC (Pando and Hernandez 2013), so we'd expect the joint stiffness to increase during our study by a factor less than 13. Contracting the main pronator and/or supinator muscles (pronator quadratus, pronator teres, supinator, and biceps brachii) only increases the K_{pp} element of the stiffness matrix. In contrast, because the main wrist muscles (flexor carpi radialis and ulnaris, extensor carpi radialis longus and brevis, and extensor carpi ulnaris) cross the radioulnar joint in addition to the wrist joint, contracting these muscles has the potential to increase each element of the stiffness matrix, including K_{pp} (see Appendix A). While the exact magnitude of this effect depends on multiple unknown factors—such as the moment arm of each muscle with respect to PS, the amount of contraction in each muscle, and the force produced by the contraction—we can identify three different cases: 1) contraction of the main pronator-supinator muscles, leading to an increase in K_{pp}, 2) contraction of the main wrist muscles, leading to an increase in the entire stiffness matrix K, and 3) contraction of the main pronator-supinator muscles and the main wrist muscles, leading to an increase in the entire stiffness matrix, but with a greater increase in K_{pp} than in the other elements. Therefore, we multiplied either K_{pp}, K, or both (K_{pp} and K) by a number of factors. For the first two cases, we multiplied K_{pp} or K by 0.5, 1, 2, 4, 6, 8, 10, 12, and 14 (the first factor, 0.5, was included in case we overestimated the passive stiffness). For the third case, we multiplied K_{pp} by these same factors but the other elements of K by the square root of these factors. Because all hypotheses except the path length hypothesis, which is purely kinematic in nature, involve joint stiffness, changes in joint stiffness have the potential to alter the prediction of all hypotheses except the path length hypothesis.

Second, we may have under- or overestimated the damping parameters. For movements not approaching the limits of the range of motion, such as the movements here, most of the joint damping is thought to arise from the same source as joint stiffness: stretching of muscles and tendons. Therefore, contracting pronator-supinator and/or wrist muscles should affect the joint damping in a similar manner as joint stiffness (the three cases mentioned above). Indeed, several studies (Dolan et al. 1993; Perreault et al. 2004; Tsuji et al. 1995) have shown that joint stiffness and damping ellipses are similar, especially in terms of orientation, which reflects the relative magnitudes of the matrix elements. Perreault further showed that increasing muscle contraction increased joint damping, but only by the square root of the increase in joint stiffness (Perreault et al. 2004). Therefore, we multiplied either D_{pp}, D, or both (D_{pp} and D), as above, but by the square root of the factors above. Changes to the damping can only affect the mechanical work and movement torque hypotheses since these are the only two hypotheses that depend on the movement and not just the final posture.

Third, we may have under- or overestimated the inertial parameters, so we multiplied either the inertia matrix I, hand mass m, or both I and m (simultaneously) by factors 0.5, 0.75, 1, 1.5, and 2. As above, changes to the inertia can only affect the mechanical work and movement torque hypotheses. However, changes to the hand mass have the potential to affect all hypotheses except the path length hypothesis.

Experiments

To measure how subjects actually combined FE, RUD, and PS during pointing movements, we performed two experiments (Experiment 1 and 2).

Experiment 1

Subjects

Twenty young, healthy, right-handed subjects (10 male and 10 female, 23±2 (mean±SD) years old, range 20-28) participated in this experiment. None of the subjects had prior knowledge of the purpose of the experiment. Subjects reported that they were free of neurological injury or biomechanical injury to the wrist or forearm. Following procedures approved by Brigham Young University's Institutional Review Board, written informed consent was obtained from all subjects.

Experimental Setup

Subjects were seated in a chair with the right arm in the parasagittal plane. The shoulder was in approximately 20° of flexion and 0° of abduction and humeral rotation, and the elbow was in approximately 30° of flexion. A shoulder belt constrained shoulder motion. The proximal 12 cm of the forearm (50% of the average forearm) rested on a horizontal support, constraining elbow motion but allowing unobstructed forearm rotation. In their right hand, subjects held a lightweight handle to which an electromagnetic motion sensor (trakSTAR by Ascension Technology Corp, Shelburne, VT) was rigidly attached. A second motion sensor was fastened to the dorsal aspect of the distal forearm, approximately 4 cm proximal to the center of the wrist joint. Together these motion sensors measured forearm pronation-supination (PS), wrist flexion-extension (FE), and wrist radial-ulnar deviation (RUD) at approximately 300Hz with an angular accuracy of 0.5° and an angular resolution and 0.1°. At a combined weight of approximately 75g, the handle and two sensors added only roughly 4% of the average total mass of the hand and forearm.

In front of the subject was a monitor with 16 peripheral targets equally distributed around a center target (Figure 1). Also displayed was a cursor that represented the direction in which the hand pointed, similar to the projection of a laser pointer on a screen. The position of the cursor on the screen was calculated from subjects' PS, FE, and RUD angles using equations 1-2 above. The cursor landed in the center target when the wrist and forearm were in neutral position, defined as follows. The forearm was in neutral PS when the dorsal aspect of the distal forearm (more specifically the dorsal tubercle of the radius and the dorsal-most protuberance of the ulnar head) was in the parasagittal plane. The wrist was in neutral FE when the handle, the center of the wrist joint, and the midpoint between the medial and lateral epicondyles were aligned. Finally, the wrist was in neutral RUD when the center of the head of the third metacarpal, the center of the wrist joint, and the lateral epicondyle were aligned. This definition of neutral position is similar to the ISB recommendation for global wrist movements (Wu et al. 2005) except that the definition of FE was adjusted to account for the fact that subjects were holding a handle.

Protocol

Subjects were asked to move the cursor from the center target to the highlighted peripheral target. After the cursor entered the boundary of the peripheral target and spent 0.5 sec within the peripheral target, the center target lit up, inviting the subject to return to the center target. After reaching the center target and spending 0.5 sec within the center target, the next peripheral target lit up, and so on. Targets were presented in pseudo-random order. No instruction was given regarding how to combine the three DOF.

To test the effect of movement distance and speed on any patterns, if they existed, the first set of 10 subjects made movements of two distances and speeds, as in the simulations. More specifically, subjects participated in four sessions. In each session, the distance from the center target to peripheral targets was either 15° or 22.5°, and subjects were instructed to move either at a comfortable pace or as fast as possible (referred to below as small, large, slow, and fast, respectively). To prevent overexertion, the sessions with the small movement distance were performed on one day, and the sessions with the large movement distance on a later day. The sessions involving the small movement distance required 15 visits to each of the 16 peripheral targets, and the sessions involving the large movement distance required 10 visits to each peripheral target. On each day, the order of the sessions (comfortable pace or as fast as possible) was randomized, with a 5-minute break between sessions.

The second set of 10 subjects only participated in two sessions. To explain, a preliminary analysis of the data from the first set of 10 subjects revealed that speed did not have a significant effect on the pattern of PS behavior. However, while most of these subjects showed a clear pattern of variation in PS with target location, there was quite a bit of inter-subject variability in the phase of the patterns, and a few subjects' data included large intra-subject variability or outliers, making it difficult to discern a consistent pattern across all subjects. Therefore, we recruited the second set of 10 subjects and asked them to make comfortably paced movements to targets at 15° (session 1) or 22.5° (session 2). In other words, the second set of 10 subjects did not make any fast movements. Both sessions required 10 visits to each of the 16 targets.

Data processing

Our analysis focused on outbound movements, i.e. movements from the center target to a peripheral target. Because each outbound movement started at the center target, where the wrist is in neutral FE and RUD position, there was no systematic drift in FE and RUD over the duration of a session. In contrast, the center target made no requirement on PS (see Kinematics above), so there was no ground reference for PS, and subjects slowly drifted in PS over the course of a session (usually toward pronation, as shown in Figure 3). Therefore, determining the amount of PS associated with an individual movement (Δp) required subtracting the PS position at the beginning of the movement (p_i) from the PS position at the end of the movement (p_f), i.e. $\Delta p = p_f - p_i$, where the beginning and end of a movement were defined as the moments the target turned on and off, respectively (see Protocol). Likewise, determining the orientation of the target (relative to the subject's rotated internal joint frame) required taking into account the PS position at the beginning of the movement (Figure 3). More specifically, we expressed the orientation of the peripheral target in terms of the subject's starting orientation, i.e. $\theta = \phi + p_i$, where ϕ is the angle of the target expressed in the external frame (x_s, y_s), and θ is the angle of the target expressed in the internal joint frame (f, u). Values of θ of 0°, 90°, 180°, and 270° correspond to targets in pure radial deviation, extension, ulnar deviation, and flexion, respectively. Note that while ϕ is one of 16 discrete angles (0°, 22.5°, 45°, …, 337.5°), θ can be any angle because p_i can be any angle.

All of the hypothesized control strategies described above predicted similar behavior in FE and RUD (see Results), so FE and RUD could not be used to discern which control strategies subjects may have used. In contrast, different hypothesized control strategies predicted significantly different behavior in PS, so we focused on PS and performed additional data processing. The amount of PS per movement (Δp) appeared to vary sinusoidally with the target angle (θ) (see Results), so we fit a sinusoidal fit to the data from each session of each subject. More specifically, we removed the bias (mean value of Δp) and performed a least-squares sinusoidal fit of the form $\Delta p = A \sin(B\theta + C)$, where A is the amplitude, B is the frequency, and C is the phase. In other words, A, B, and C became the measures describing the pattern of behavior in PS that we used in our statistical analysis (see below). The goodness of fit was determined as the R-value of each fit. The mean fit was defined as $\Delta p = \bar{A} \sin(\bar{B}\theta + \bar{C})$, where $\bar{A}$, $\bar{B}$, and $\bar{C}$ were the mean of A, B, and C across subjects.

Statistical analysis

The resulting data describing the behavior in PS included three measures (A, B, and C) and three factors: distance (small and large), speed (slow and fast), and subject (1-20). There were a total of 60 factor-level combinations: 2*2 for the first set of 10 subjects and 2*1 for the second set of 10 subjects (only the first set of subjects performed fast movements—see above). Any factor-level combination for which A, B, or C was more than 2 standard deviations from the mean was considered an outlier and excluded from further analysis.[5] On the remaining data set we performed for each measure a three-way mixed-model ANOVA with factors distance, speed, and subject, with subject as a random factor.

Experiment 2

In Experiment 1, subjects began each movement in neutral FE and RUD, but PS was not constrained to start in neutral PS. This difference in the initial states of the DOF could have affected how subjects controlled the DOF. To test this hypothesis, we repeated Experiment 1, but with PS constrained to start in neutral position so all three DOF would have the same initial conditions.

Ten new, healthy, right-handed subjects (5 male and 5 female, 26±13 years old, range 18-54) participated in Experiment 2. As in Experiment 1, none of the subjects had prior knowledge of the purpose of the experiment, and subjects reported that they were free of neurological injury or biomechanical injury to the wrist or forearm. Following procedures approved by Brigham Young University's Institutional Review Board, written informed consent was obtained from all subjects.

The setup, protocol, and data processing of Experiment 2 were identical to those of Experiment 1 except for the following differences. 1) We added to the cursor two crosshairs (i.e. two sets of mutually perpendicular lines) that translated with the cursor. The crosshairs were centered in the center of the cursor and extended a bit beyond the circumference of the cursor. As the crosshairs translated with the cursor, one always remained vertical and horizontal, whereas the other rotated with PS. Therefore, the angle between the crosshairs represented the amount of PS. When the crosshairs were aligned, the forearm was in neutral PS. For the next peripheral target to appear, subjects had to bring the cursor to the center target and (at the same time) align the crosshairs, requiring all three DOF to be in neutral position at the start of each movement. The tolerance was equal for all three DOF: to bring the cursor within the center target required FE and RUD to be within 1.5° of their neutral positions, and the crosshairs were required to be aligned within 1.5° of each other, forcing PS to be within 1.5° of its neutral position. Both crosshairs appeared only when the cursor was within the center target; once the movement was underway and the cursor left the center target, the crosshairs vanished to avoid any suggestion that subjects should continue to maintain the forearm in neutral PS. 2) Having determined in Experiment 1 the effect of movement amplitude and speed, we focused here on testing the effect of controlling the initial state of PS. Therefore, subjects only made small-slow movements, visiting each of the 16 targets 10 times.

To determine the effect of constraining PS at the center target (at the beginning of the movement), we compared Δp between the small-slow movements of the subjects in Experiment 1 (where PS was not constrained at the center target) and the small-slow movements of the subjects in Experiment 2 (where PS was constrained at the center target). More specifically, we performed for each measure (amplitude, frequency, and phase) a two-way mixed-model ANOVA with factors constraint (unconstrained or constrained) and subject, with subject as a random factor.

---

[5] We used 2 SD because several extreme outliers skewed the mean and SD of the relatively small sample size (one fit per subject, resulting in only 10 samples for some protocols) to the point that they were still within 3 SD even though they clearly different from the rest of the data.

Comparison of Experimental and Simulated Data

We compared the pattern of Δp vs. θ predicted by each hypothesis to the observed pattern in terms of shape (e.g. sinusoidal), frequency, amplitude, and phase. Since most of the hypotheses exhibited patterns of Δp that were not sinusoidal (see Results), we used the following definitions. Frequency was defined as the number of local maxima per revolution in θ, and amplitude was defined as half the difference between the global maximum and global minimum of Δp. The phase was defined as for a sinusoid, i.e. $90° - B\theta_{max}$, where B is the frequency of Δp and θ_{max} is the value of θ at which the first local maximum in Δp occurs.

Results

Simulations

All of the hypothesized control strategies predicted similar behavior in FE and similar behavior in RUD (Figure 4A-B). This behavior is expected for a task that is most sensitive to FE and RUD: pointing up used mostly radial deviation, pointing right used mostly extension, pointing down used mostly ulnar deviation, and pointing left used mostly flexion (**Figure 1**). In contrast, the predicted behavior in Δp varied greatly between hypotheses (Figure 4C). Amplitudes ranged from 1° (path length) to 23° (postural torque), frequencies were either 1 cycle/rev (simplifying strategy) or 2 cycles/rev (all other hypotheses), and phase ranged from 34° (mechanical work) to 180° (path length). Because different hypothesized control strategies predicted significantly different behavior in PS, we focused on the predicted behavior in PS (as opposed to FE or RUD) to discern which control strategies subjects may have used. As mentioned above, we repeated the simulations for two movement distances and speeds, but all hypotheses showed the same effect: increasing the distance to the peripheral targets increased the amplitude of Δp, and increasing movement speed had no effect on Δp.

Sensitivity Analysis

As described above, we also repeated the simulations with different model parameters (stiffness, damping, inertia, and mass) to determine the effect on the predicted behaviors in PS. A detailed report can be found in the Appendix B. Summarizing, we found that: 1) The frequency of the Movement Torque and Postural Torque hypotheses varied between 1, 2, and 3 cycles/rev depending on stiffness, whereas the frequencies of the other hypotheses were constant at 1 cycle/rev (Simplifying Strategy) or 2 cycles/rev (Mechanical Work, Potential Energy, and Path Length) regardless of stiffness, damping, or inertia/mass. 2) The amplitude of hypotheses were most sensitive to stiffness; except for the Path Length hypothesis, the amplitudes of all hypotheses decreased dramatically with increases in the stiffness in PS (K_{pp}). In contrast, increasing damping only affected the Mechanical Work and Movement Torque Hypotheses (modest decrease in amplitude), changing inertia had virtually no effect on any hypothesis, and increasing hand mass caused only a modest increase or decrease in some hypotheses.

Experiments

Experiment 1

Subjects' pointing movements consisted mostly of FE and RUD, as expected for a task that is most sensitive to these two DOF (Figure 5A). In harmony with the simulations described above, FE and RUD varied sinusoidally with movement direction: subjects used mostly radial deviation, extension, flexion, and ulnar deviation for pointing up, right, down, and left, respectively (Figure 1). As explained above, PS drifted over the course of the experiment (**Figure 3**A). This behavior in FE, RUD, and PS was previously described in detail (Campolo et al. 2009; Campolo et al. 2010; Campolo et al. 2011). In contrast, the *change in PS* during each movement (Δp), which was much smaller in comparison, has not been reported previously and proved valuable in discerning between control strategies. Most subjects exhibited a discernible sinusoidal pattern in Δp vs. θ (Figure 6A). For example, averaged over the small-slow session, the sinusoidal fits of Δp with respect to θ had an amplitude of 1.52° ± 0.66° (mean ± SD), a frequency of 1.04 ± 0.08 cycles per revolution in θ, a phase of 138° ± 36° (relative to a pure sinusoid), and an average correlation coefficient (R-value) of 0.77 ± 14 (Table 1).

This sinusoidal pattern in Δp vs. θ persisted despite changes in movement speed or distance, though increasing the distance did increase the amplitude of the sinusoidal pattern ($p<0.001$; Table 2): on average, increasing the distance between targets by 50% (from 15° to 22.5°) increased the amplitude of Δp by 100% (from 1.6° to 3.2°). There were several other statistically significant effects, but the effect sizes were small. Distance and speed had statistically significant main and interaction effects on the frequency of Δp (Table 2), but the average frequency remained close to 1 cycles per revolution in θ (range 0.84-1.05 cycles/rev) for all factor-level combinations (small, large, slow, and fast). Unless there is an unexplainable discontinuity in Δp at $\theta = 0°$ (radial deviation), the frequency of Δp must be an integer number of cycles per revolution in θ, so we interpreted the fit frequencies to be 1 cycle/rev (as opposed to 2 or 3 cycles/rev). The only other statistically significant effect was also relatively small: increasing the movement speed from a comfortable pace to "as fast as possible" decreased the average phase from 138° to 127°. There were no statistically significant effects of distance or speed on the correlation coefficient R. Because the pattern in Δp vs. θ was similar for both distances and speeds, we present the results only for the small-slow condition.

Experiment 2

As in Experiment 1, subjects in Experiment 2 pointed mostly using FE and RUD, with little movement in PS by comparison (Figure 5B). Also as in Experiment 1, most subjects' small movement in PS exhibited a discernible sinusoidal pattern in Δp vs. θ (Figure **6**B). Averaged over all 10 subjects (Figure **7**C), the sinusoidal variation of Δp with θ had an amplitude of 2.45° ± 1.22° (mean ± SD), a frequency of 1.04 ± 0.04 cycles per revolution in θ, a phase of 136° ± 28° (relative to a pure sinusoid), and an average correlation coefficient (R-value) of 0.76 ± 08 (Table **3**).

Comparison between Experiment 1 and Experiment 2

Constraining PS at the center target increased the amplitude of Δp (p=0.007) from 1.4061° to 2.1484° but had no statistically significant effect on frequency, phase, or the correlation coefficient (Table 4). In other words, constraining PS at the center target only increased the amplitude of the phenomenon (the pattern in Δp).

Comparison of Experimental and Simulated Data

As the effect of movement distance and speed was the same for all hypothesized control strategies and similar to the effect on the observed behavior (increasing distance increases Δp, but increasing speed does not affect Δp), we could not use this effect to determine which control strategy best matched the observed behavior. Instead we turned to the change in Δp with movement direction (Figure 8A). A comparison of the experimental data to the first set of simulations (using the default model parameters) shows that none of the predicted patterns in Δp matched the observed pattern in amplitude, frequency, and phase. However, under certain conditions within the physiologically plausible range of parameter variations (see Methods), three hypotheses matched the experimental data in amplitude, frequency, and phase: Simplifying Strategy, Movement Torque, and Postural Torque (Figure 8B).

The Simplifying Strategy hypothesis matched the experimental data most closely and most robustly. Its predicted pattern of Δp was always sinusoidal with a frequency of 1 cycle/rev regardless of parameter values, but the amplitude predicted with the default parameters was too high. However, the amplitude decreased if K_{pp} or both K_{pp} and K were increased. The predicted amplitude perfectly matched the observed amplitude when K_{pp} was increased by a factor of 3.7 or K_{pp} and K were increased together (K_{pp} by a factor of 7.8 and the other elements of K by a factor of 2.8). Increasing K_{pp} caused the predicted phase (131°) to match the observed phase (138±36°) more closely than increasing K_{pp} and K together (100°).

Although the Movement Torque hypothesis was never exactly sinusoidal and varied in frequency between 1, 2, and 3 cycles/rev, there existed a narrow window of parameter values in which its predicted pattern matched the observed pattern quite closely: if K_{pp} was multiplied by a factor of 5.8, the predicted pattern was roughly sinusoidal with a frequency of 1 cycle/rev, amplitude of 1.5°, and phase of 123° (Figure 8B). Likewise, the Postural Torque hypothesis was never exactly sinusoidal and also varied in frequency, but there were two conditions with an approximate match: 1) when K_{pp} was multiplied by a factor of 6.3, the predicted pattern was roughly sinusoidal with a frequency that looked like 1 cycle/rev (it was actually 2 cycles/rev, but one of the maxima was small), amplitude of 1.5°, and phase of 137°; and 2) when K_{pp} and K were increased together (K_{pp} by a factor of 14 and the other elements of K by a factor of $\sqrt{14}$), the predicted pattern was roughly sinusoidal with a frequency of 1 cycle/rev, amplitude of 2.2°, and phase of 111°. Note that the mean of the experimental data was removed before fitting it with sinusoids (see Methods), so the difference in absolute value between the experimentally observed pattern and these hypotheses should be ignored.

Of these three hypotheses, the Simplifying Strategy hypothesis is the most likely cause of the observed pattern in Δp for two reasons. First, its pattern matches the observed pattern far more robustly than the other two hypotheses. The Simplifying Strategy hypothesis always exhibits the same shape (sinusoidal) and frequency as the observed data, as well as a similar phase, independent of model parameters. Although not all of the experimental data sets exhibited a clear sinusoidal pattern with a frequency of 1 cycle/rev (Figure 6), none of the sets exhibited discernable patterns with frequencies other than 1 cycle/rev. Second, the change in model parameters required to achieve a close match in amplitude as well (i.e. increasing K_{pp} by a factor of 3.7) is one that is entirely plausible; using co-contraction to stabilize a proximal DOF (PS) against interaction torques created during a movement planned to involve only distal DOF (FE and RUD) is a reasonable strategy. In contrast, the Movement Torque and Postural Torque hypotheses do not consistently match the observed behavior. These hypotheses exhibit patterns that differ from the observed behavior in shape, frequency, amplitude, and phase for much of the physiologically plausible range of model parameters. Only in a relatively narrow window of model parameters do the predicted patterns match the observed pattern. Perhaps most importantly, the changes in model parameters required to make the predicted patterns match the observed pattern are unlikely to occur in the context of these two hypotheses. In other words, there is no a priori reason why the Movement Torque or Postural Torque hypotheses should include a stiffening of the PS DOF that is significantly higher than the stiffening that might occur in FE or RUD. We therefore concluded that the Simplifying Strategy hypothesis is the most likely hypothesis, and we performed additional tests to further probe the match between the predicted and observed patterns.

Further Testing of the Simplifying Strategy Hypothesis

While the phase predicted by the simplifying strategy hypothesis (131°) matched the experimentally observed phase on average (138°), the latter exhibited considerable variability between subjects (SD = 36°; range = 44°-188°; Figure 7A). To test whether the simplifying strategy hypothesis could predict this large variability between subjects, we determined the effect of inter-subject variation in modeling parameters on the predicted phase by repeating the simulation of the Simplifying Strategy Hypothesis using the individual inertia, damping, and stiffness matrices of ten young, healthy subjects (five male and five female) who participated in a prior study (Peaden and Charles 2014). Although these subjects were not the same subjects who participated in our study, the variation in their inertia, damping, and stiffness was assumed to be similar to the variation in the subjects who participated in our study (for whom individual parameters were unknown). We found that the variation in predicted phase produced by using individual inertia, damping, and stiffness matrices (SD = 24°; range = 95°-166°) was of the same order of magnitude as the variation in phase observed experimentally, providing another indication that the simplifying strategy hypothesis could be the cause of the observed pattern of Δp.

Discussion

Pointing with the three DOF of the wrist and forearm (PS, FE, and RUD) is a component of many everyday manipulation tasks in which the long axis of an object needs to be oriented in a particular way. Although this task is more sensitive to FE and RUD than to PS and could be accomplished using FE and RUD alone, Campolo et al found that subjects tended to use a small amount of PS (Campolo et al. 2009; Campolo et al. 2010; Campolo et al. 2011). The goal of this study was to uncover the reason subjects pointed in this manner. We tested a variety of common cost functions and found that minimizing these cost functions did not predict the observed behavior. In contrast, an alternative hypothesis, stipulating that subjects planned pointing movements using only FE and RUD, and that the observed movement in PS was just a side-effect of unopposed interaction torques, fit the data closely and robustly. Therefore, we concluded that humans tend to control moderately sized pointing movements involving the wrist and forearm by ignoring the forearm.

Context

The conclusion that subjects focused on the most important DOF and ignored the least important DOF may not seem very interesting unless one considers the full picture. First, according to our simulations, the control strategy of ignoring the forearm does not minimize energy, work, torque, or path length. For many redundant tasks, the observed behavior can be predicted using a variety of different cost functions, making it difficult to discern which cost function (or combination of cost functions) may have been minimized. In contrast, for the pointing task studied here, only one of the control strategies tested predicted the observed behavior robustly. This is a strong result; not only does it clearly favor the simplifying strategy hypothesis, it also implies that the cost functions associated with torque, energy, work, and path length were not minimized. We conclude that, for this specific task, the control system either a) values simplicity in control ("control the most important DOF and ignore the others") more than minimizing torque, energy, work, or path length, b) does not perceive a difference in cost, i.e. the difference in cost may be below the perceptual threshold, or c) does not know how to minimize the other costs.

Second, although PS affects the task goal less than FE and RUD, it still affects it, and ignoring PS results in movement error. To clarify, ignoring PS in the planning stage results in unopposed interaction torques in the execution stage; these unopposed interaction torques in turn produce movement in PS, resulting in simulated mean and maximum errors in pointing direction of 1.2° and 2.7°, respectively. Although these errors are relatively small (the targets had a radius of 1.5°), the fact that these errors went unchecked during the duration of the experiment implies that the increase in simplicity with this control strategy (ignoring PS) was worth the decrease in accuracy.

Third, the conclusion that subjects focused on the most important DOF and ignored the least important DOF goes far beyond (if not differs from) the conclusion of previous investigations of this task, which stated that the observed pattern was due to a neural constraint. Following Donders' approach (for a summary, see (Campolo et al. 2010)), Campolo et al focused their analysis on the rotation axis that transforms the wrist and forearm from their neutral position to a given orientation (Campolo et al. 2009; Campolo et al. 2010; Campolo et al. 2011; Tagliamonte et al. 2011). They found that the coordinates of this rotation axis tend to lie on a 2-D subspace (a surface) of the 3-D space of the vector, indicating that subjects' behavior followed Donders' Law. Following similar investigations of Donders' Law in eye movements, Campolo et al concluded that this (the fact that subjects' behavior followed Donders' Law) implied the existence of a neural constraint on the kinematics of wrist and forearm rotations.

Donders' Law

Does the observed pattern follow Donders' Law? It depends on the definition since Donders' Law has been variously used to describe both phenomena and control strategies (Ceylan et al. 2000; Crawford et al. 2003; Ghosh and Wijayasinghe 2012; Gielen et al. 1997; Glenn and Vilis 1992; Hore et al. 1994; Hore et al. 1992; Kunin et al. 2007; Liebermann et al. 2006a; Liebermann et al. 2006b; Marotta et al. 2003; Radau et al. 1994; Soechting et al. 1995; Thurtell et al. 2012; Tweed 1997). To clarify, Donders' Law can be defined as a description of an experimentally observed phenomenon, similar to Fitts' Law (Fitts 1954) or the Two-third Power Law (Lacquaniti et al. 1983; Viviani and Schneider 1991). These laws describe experimentally observed relationships (invariants or stereotyped behaviors) between variables that are not fully constrained by the movement task. Specifically, Donders' Law describes the existence of a kinematic relationship between redundant rotational DOF. Because Δp is a function of PS, and θ is a function of target position (x_s, y_s), which in turn is a function of PS, FE, and RUD (by Equations 1 and 2), the observed sinusoidal relationship between Δp and θ implies a relationship between PS, FE, and RUD. This latter relationship can be expressed alternatively as a relationship between the coordinates of the rotation vector (by expressing PS, FE, and RUD as a rotation matrix and calculating the rotation vector from the matrix (Craig 2005)). Therefore, if Donders' Law is defined as an experimentally observed relationship between rotation vector coordinates, then the pattern of behavior described in this paper qualifies as an instance of Donders' Law, as would any other kinematically redundant rotation that exhibits stereotyped kinematics.

Alternatively, Donders' Law is sometimes interpreted as a neural constraint on joint kinematics used to solve the redundancy problem. This interpretation is in our view problematic because the observation of a pattern between redundant kinematic variables does not necessarily imply a control strategy that directly constrains these variables. Such a pattern may instead result from higher-order control strategies that do not directly place any constraints on these kinematic variables. For example, we have proposed in this paper that the observed pattern of PS is not directly controlled but rather a mechanical side effect of a control strategy that focuses on FE and RUD.

Simplifying strategies

The hypothesis that humans employ simplifying strategies instead of optimization is not new and has found traction in a variety of fields. For example, referring to economic decision making, Simon observed in 1956 that "however adaptive the behavior of organisms in learning and choice situations, this adaptiveness falls far short of the ideal of "maximizing" postulated in economic theory. Evidently, organisms adapt well enough to "satisfice"; they do not, in general, "optimize."" (Simon 1956). Similar simplifying strategies have been hypothesized for controlling movement: "the individual confronted with a new task has no motivation to find a solution that is optimal according to physical performance criteria; rather, the motivation is to find quickly a solution that is good enough to get rewarded without expending more time or effort than the reward is perceived to be worth" (Loeb 2012). In their experiment with multiple local cost-function minima, Ganesh et al observed that subjects frequently chose a suboptimal solution "even after sufficient experience of the optimal solution" (Ganesh et al. 2010). Such "good-enough control" strategies often enjoy a robust multiplicity of solutions that could be acquired via trial-and-error learning instead of the more mathematically complex process of optimization.

The passive motion paradigm (PMP) has been proposed as an alternative to optimal control (Mohan and Morasso 2011) and was recently applied to the problem of pointing with the wrist and forearm (Tommasino and Campolo 2017). This strategy "offers the brain a way to dynamically link motor redundancy with task-oriented constraints "at runtime," hence solving the "DoFs problem" without explicit kinematic inversion and cost function computation" (Mohan and Morasso 2011). The basic idea is that task goals are reformulated as attractor fields that pull the end-effector toward the goal, naturally resulting in joint displacements that satisfy the dynamic constraints imposed by joint impedance, including interaction torques.[6] The

[6] To clarify, the "DoFs problem" can be stated as follows: given a task goal (e.g. move the end-effector from A to B), what must the joints do to achieve this goal? If the linkage is

simplifying strategy proposed here shares some similarity to the PMP but differs in a key aspect: instead of the end-effector (x_s and y_s) being attracted toward the target, it is a subset of the joint DOF (FE and RUD) that is "attracted" (actually constrained to follow a straight-line trajectory) toward the target. One could argue that constraining these DOF to follow a straight-line trajectory toward the target effectively constrains the end-effector to follow a straight-line trajectory toward the target as well (because the position of the end-effector is more sensitive to FE and RUD than to PS—see Methods). However, this kinematic constraint is very different from the dynamic constraints imposed by the impedance. Consequently, the PMP will predict movements that are, in general, different from those predicted by the simplifying strategy proposed here.

Our conclusion that FE and RUD are controlled while PS is ignored bears some resemblance to the leading-joint hypothesis (LJH), a simplifying strategy for controlling the dynamics of multi-joint movements according to the hierarchy of the joints (Dounskaia 2005). The "leading" joint is accelerated or decelerated "as during single-joint movements, i.e. largely disregarding motion at the other joints," whereas the subordinate joints are left to "regulate interaction torque [created by the motion of the leading joint] and to create net torque that results in motion of the end-effector required by the task" (Dounskaia 2005). However, we observed two "leading joints" (FE and RUD), not one, and we did not observe any regulation of interaction torques by the subordinate joint (PS), although it is possible that such regulation would have occurred if the effect on PS had been large enough to interfere with the task.

Whether the particular simplifying strategy we observed is applied to other kinematically redundant tasks no doubt depends on the task, the DOF involved, the size of the task movements relative to the range of movement in each DOF, speed and accuracy constraints, etc. For example, if we had placed the targets in our task beyond the range of motion in radial-ulnar deviation (e.g. beyond ±30°), subjects would not have been able to ignore PS and accomplish the task with FE and RUD alone—they would have been forced to use a different control strategy that involved a large amount of PS.

---

kinematically redundant (i.e. if the number of joint DOF exceeds the number of task goal constraints), this question does not have a unique solution (the Jacobian cannot be inverted). A common approach is to add constraints (such as a cost function that must be minimized) to ensure a unique solution (to make the Jacobian invertible). Instead, the PMP puts this approach on its head by formulating the task goal in terms of an attractor force field: the end-effector is attracted toward the goal (e.g. from A to B). The key is that applying a force to the end-effector creates torques at the joints that are well-defined, even for a kinematically redundant linkage (whereas the transformation of kinematics is well-defined from joint space to task space, the transformation of force/torque is well-defined from task space to joint space). Well-defined joint torques lead naturally to joint displacements, "analogous to the mechanism of coordinating the motion of a wooden marionette by means of strings attached to the terminal parts of the body: the distribution of the motion among the joints is the "passive" consequence of the virtual forces applied to the end-effectors and the "compliance" [admittance, i.e. the inverse of mechanical impedance] of different joints" (Mohan and Morasso 2011). Finally, joint displacements result in end-effector displacements toward the goal. Thus, the PMP suggests that instead of planning a movement by minimizing a cost function, subjects "imagine" (animate) the end-effector being pulled toward the goal and "observe" the resultant joint displacements, and then implement these joint displacements to execute the movement.

That said, our finding that some of the observed behavior was caused by mechanics may hold true in other tasks as well. It is not uncommon to discover that behavior previously ascribed solely to a neural constraint is caused, at least in part, by the mechanics of the "plant". For example, whereas early investigations of eye movement behavior postulated that the problem of noncommutativity of ocular rotations was solved within neural networks, more recent investigations found that "part of the solution for kinematically appropriate eye movements is found in the mechanical properties of the eyeball" (Ghasia and Angelaki 2005). Such mechanical properties often include lower-level anatomical constraints that naturally favor some patterns of joint rotation between DOF, sometimes termed non-independence (for example the non-independence of finger action). One way to represent non-independence is through interaction torques, which specify the torque in one DOF due to displacement, velocity, acceleration, etc., in other DOF. In a linear model, interaction torques stem from the off-diagonal terms of the stiffness, damping, and inertia matrices, which are precisely the linear approximation of non-independence constraints. A few past studies have characterized the coupled stiffness, damping, and inertia matrices of these three DOF (Drake and Charles 2014; Park et al. 2017), and since our model includes these matrices, it includes a linear approximation of the non-independence between these three DOF. Furthermore, our conclusion that the behavior in PS is due to uncontrolled interaction torques is the same as the conclusion that the behavior in PS is due to non-independence between the three DOF. Thus the behavior in PS is not a control strategy; PS is *uncontrolled*. However, the choice to control the pointing direction using only FE and RUD and not PS, as well as the choice to leave PS exposed to interaction torque without intervention, can be considered part of the control strategy.

Limitations

We modeled the pointing movements using a relatively simple joint-level model because it allowed us to test a large variety of control strategies. Although this model includes the first-order muscle mechanics felt at the joint level (see Methods), it ignores many other effects included in state-of-the-art musculoskeletal modelling software, such as non-linearities in the muscle force-length and force-velocity effects, changing moment arms, and muscle activation dynamics. Including these effects may have yielded different results, but such modelling software does not allow direct investigation of the control strategies investigated here and relies on a large number of model parameters, making it difficult to discern the robustness of results. Because the model used here was simple, it provides—to the best of our knowledge—the simplest explanation of the observed behavior.

We tested a relatively large and diverse set of hypotheses involving work, potential energy, torque during movement, torque required to maintain a posture, path length, and simplifying strategy. The simplifying strategy hypothesis matched the observed pattern in frequency and phase and, if the stiffness was increased in a plausible manner, amplitude as well. In contrast, the other hypotheses failed to robustly match the observed behavior in one or more significant aspects. We therefore concluded that the observed behavior in PS was due to mechanical coupling. Nevertheless, it is possible that other plausible but untested hypotheses could match the data as well. Such plausible hypotheses include combinations of the cost functions tested here (Berret et al. 2011). That said, combining multiple cost functions with different weightings introduces more unknown variables, making it difficult to determine the strategy that is actually employed.

The observed displacement in PS was small (mean amplitude of 1.4° for small, slow movements), and it is possible that the pattern was affected or even caused by soft-tissue artifact. It is difficult to completely rule out this possibility without measuring the movement of the bones directly. Nevertheless, the simplicity of the hypothesis that the neuromuscular system solves the problem of redundancy in pointing with the forearm and wrist by focusing on the most task-relevant DOF, combined with the fact that it fits the observed pattern quite well, argues in favor of our conclusion.

The conclusions of this paper should not be extrapolated beyond the conditions tested here, in particular to rotations of much larger amplitude. The current study focused on rotations of moderate size (15° and 22.5°). In this space, the only hard constraint on the three DOF (PS, FE, and RUD) is that the hand point toward the target (i.e. Equations 1-2). Even though 22.5° was close to subjects' available ROM in radial deviation, all subjects were able to reach the target in radial deviation without significant use of PS. In other words, the observed pattern of PS did not serve to rotate subjects' wrist toward flexion or extension in order to take advantage of the larger ROM in FE; the amplitude in PS was on average 1.52° (Table 1), which is far too small to gain an effective increase in ROM. That said, if targets were placed beyond the available ROM in RUD (e.g. at 45°), subjects would be forced to adopt the strategy of using large rotations in PS to allow them to reach otherwise unattainable targets (i.e. those close to the y_s-axis) with FE instead of RUD. Also, as the distance to the target increases, the role of PS increases. In other words, as the distance to the target increases, poorly controlling PS increasingly deteriorates the accuracy of the pointing direction. Therefore, although interaction torques on the forearm exist for any non-trivial rotation, other factors become increasingly important for larger rotations, so it is unlikely that the conclusions reached in this paper would extrapolate to pointing movements requiring much larger rotations. That said, the rotations investigated here are relevant since rotations of this size (up to 22.5°) cover approximately 70% of the range of motion used during activities of daily living (Anderton and Charles 2012).

All subjects performed the task with their right upper limb. We expect the pattern of Δp for the left limb to be identical to the pattern for the right limb when the pattern is expressed in joint space. For example, a movement of the right limb involving extension and radial deviation should elicit the same amount of Δp as a movement of the left limb involving extension and radial deviation. However, we expect to see a difference between limbs when Δp is mapped onto target angles (i.e. a plot of Δp vs. θ) since extension and radial deviation move the right hand toward a target in the first quadrant but the left hand toward a target in the fourth quadrant. Therefore, we expect the pattern of Δp vs. θ for the left limb to be reflected about $\theta = 180°$ relative to the pattern of Δp vs. θ for the right limb.

Conclusion

How the neuromuscular system deals with kinematic redundancy is an important question in motor control and has been the focus of many studies. However, although the wrist and forearm are known to combine in a stereotyped pattern during kinematically redundant pointing movements (Campolo et al. 2009; Campolo et al. 2010; Campolo et al. 2011), the reason the neuromuscular system selects this pattern has been unknown. Here we presented the key observation that in many subjects pronation-supination (PS) varied sinusoidally with target direction, and we tested a variety of hypothesized reasons underlying this pattern. The hypotheses involving common cost functions failed to robustly predict the observed behavior, while the hypothesis that the pointing movement is planned using only FE and RUD predicted behavior that matched the observed pattern quite well, especially when stiffness was increased in a plausible manner. We conclude that the neuromuscular system solves the challenge of kinematic redundancy in moderately-sized pointing movements involving the wrist and forearm by ignoring the forearm even though this strategy does not robustly minimize work, potential energy, torque, or path length.

Appendix A

The relationship between joint stiffness and muscle stiffness depends on the Jacobian between joint space and muscle space (Burdet et al. 2013). Joint space is defined by joint angles $\vec{q} = [p, f, u]^T$. Muscle space is defined by muscle lengths $\vec{\lambda} = [\lambda_1, \lambda_2, \dots, \lambda_8]^T$, where muscles 1-4 represent the main pronator-supinator muscles (pronator quadratus, pronator teres, supinator, and biceps brachii), and muscles 5-8 represent the main wrist muscles (flexor carpi radialis, flexor carpi ulnaris, extensor carpi radialis longus and brevis (combined), and extensor carpi ulnaris).

The relationship between muscle velocity and joint speed is given by the moment arms ρ_{ij} between muscle i and joint coordinate j:

$$\begin{bmatrix} \dot{\lambda}_1 \\ \dot{\lambda}_2 \\ \dot{\lambda}_3 \\ \dot{\lambda}_4 \\ \dot{\lambda}_5 \\ \dot{\lambda}_6 \\ \dot{\lambda}_7 \\ \dot{\lambda}_8 \end{bmatrix} = \begin{bmatrix} \rho_{11} & 0 & 0 \\ \rho_{21} & 0 & 0 \\ \rho_{31} & 0 & 0 \\ \rho_{41} & 0 & 0 \\ \rho_{51} & \rho_{52} & \rho_{53} \\ \rho_{61} & \rho_{62} & \rho_{63} \\ \rho_{71} & \rho_{72} & \rho_{73} \\ \rho_{81} & \rho_{82} & \rho_{83} \end{bmatrix} \begin{bmatrix} \dot{p} \\ \dot{f} \\ \dot{u} \end{bmatrix}$$

The matrix of moment arms is the Jacobian J_μ that transforms the matrix of muscle stiffness, K_μ, into the matrix of joint stiffness, K (Burdet et al. 2013):

$$K = {J_\mu}^T K_\mu J_\mu + \frac{d{J_\mu}^T}{d\vec{q}} \vec{\mu}$$

where $\vec{\mu}$ is the 7-element vector of muscle forces corresponding to $\vec{\lambda}$. Assuming that the stiffness of each muscle is independent from the stiffness of the other muscles (i.e. assuming K_μ is diagonal), and focusing on the relationship between muscle stiffness and joint stiffness (i.e. ignoring the second term on the right), the elements of K are:

$$K(1,1) = K_\mu(1,1){\rho_{11}}^2 + K_\mu(2,2){\rho_{21}}^2 + K_\mu(3,3){\rho_{31}}^2 + K_\mu(4,4){\rho_{41}}^2 + K_\mu(5,5){\rho_{51}}^2 + K_\mu(6,6){\rho_{61}}^2 + K_\mu(7,7){\rho_{71}}^2 + K_\mu(8,8){\rho_{81}}^2$$

$$K(1,2) = K_\mu(5,5)\rho_{51}\rho_{52} + K_\mu(6,6)\rho_{61}\rho_{62} + K_\mu(7,7)\rho_{71}\rho_{72} + K_\mu(8,8)\rho_{81}\rho_{82}$$

$$K(1,3) = K_\mu(5,5)\rho_{51}\rho_{53} + K_\mu(6,6)\rho_{61}\rho_{63} + K_\mu(7,7)\rho_{71}\rho_{73} + K_\mu(8,8)\rho_{81}\rho_{83}$$

$$K(2,1) = K(1,2)$$

$$K(2,2) = K_\mu(5,5){\rho_{52}}^2 + K_\mu(6,6){\rho_{62}}^2 + K_\mu(7,7){\rho_{72}}^2 + K_\mu(8,8){\rho_{82}}^2$$

$$K(2,3) = K_\mu(5,5)\rho_{52}\rho_{53} + K_\mu(6,6)\rho_{62}\rho_{63} + K_\mu(7,7)\rho_{72}\rho_{73} + K_\mu(8,8)\rho_{82}\rho_{83}$$

$$K(3,1) = K(1,3)$$

$$K(3,2) = K(2,3)$$

$$K(3,3) = K_\mu(5,5){\rho_{53}}^2 + K_\mu(6,6){\rho_{63}}^2 + K_\mu(7,7){\rho_{73}}^2 + K_\mu(8,8){\rho_{83}}^2$$

It can be seen that $K(1,1)$ (also known as K_{pp}) depends on the stiffness of all muscles (1-8), whereas all other elements of K depend only on the stiffness of wrist muscles (5-8). It is readily shown that this statement holds true even if the stiffness of pronator-supinator muscles are interdependent and the stiffness of wrist muscles are interdependent (i.e. if K_μ is not diagonal) as long as the stiffness of pronator-supinator muscles are independent from the stiffness of wrist muscles, and vice versa (i.e. if the 4-by-4 submatrices in the bottom-left and top-right of K_μ are zero).

Appendix B

Stiffness: Changing stiffness affected the predicted Δp pattern of all hypotheses except the path length hypothesis. Mechanical Work and Potential Energy: Changes in the stiffness parameters affected these two hypotheses in a similar manner. Changing stiffness had no effect on the frequency of the predicted Δp; it remained at 2 cycles/rev, independent of stiffness. Increasing K_{pp} or both K_{pp} and K decreased the amplitude of the predicted Δp, whereas increasing K had little effect. For increases in K_{pp} or both K_{pp} and K, the amplitude decreased from a maximum around 14° (factor 0.5) to a minimum around 0.6° (factor 14). Movement Torque and Postural Torque: Changing stiffness had a strong effect on the shape and frequency of Δp. Increasing K_{pp}, K, or both caused the frequency of the Movement Torque hypothesis to transition from 2 cycles/rev for low factors (around 0.5 and 1) to 1 cycle/rev for intermediate factors (around 4 and 6) and then to 2 or even 3 cycles/rev for higher factors (around 8 and above). The Postural Torque hypothesis exhibited a similar transition for increases in K_{pp} but remained at 2 cycles/rev for increases in K and did not exhibit the transition from 1 to 2 cycles/rev for increases in both K_{pp} and K. Increasing K_{pp} or both K_{pp} and K decreased the amplitude of the predicted Δp, whereas increasing K had little effect. For increases in K_{pp} or both K_{pp} and K, the amplitude of the Movement Torque and Postural Torque hypotheses decreased from a maximum of 30° and 73° (factor 0.5) to a minimum of 0.7° and 0.8° (factor 14), respectively. Simplifying Strategy: Changing stiffness had no effect on the shape or frequency of Δp; it remained sinusoidal with a frequency of 1 cycle/rev regardless of stiffness. Increasing K_{pp}, K, or both decreased the amplitude of Δp. This effect was strongest for increases in K_{pp}, which caused a decrease in amplitude from 13° (factor 0.5) to 0.4° (factor 14).

Damping: As mentioned above, changes in damping can only affect the Mechanical Work and Movement Torque hypotheses since these are the only hypotheses that depend on movement. Changing damping had a similar effect on both hypotheses. The shape of both hypotheses was virtually unaffected by all changes in damping, with frequencies of 2 cycles/rev regardless of damping. Increasing D_{pp} or both D_{pp} and D decreased the amplitude of the

Mechanical Work and Movement Torque hypotheses from approximately 7° and 20° (factor 0.5) to approximately 5° and 13° (factor 14), respectively. Increasing *D* alone had virtually no effect on either hypothesis.

Inertia and mass: Changes in inertia can only affect the Mechanical Work and Movement Torque hypotheses. That said, the effect on these hypotheses was negligible; the patterns and amplitudes appeared independent of inertia. In contrast, changes in the hand mass had the potential to affect all hypotheses except the path length hypothesis. While changing the hand mass did not change the frequency of any of the hypotheses, it did change some of the amplitudes. Increasing the mass had negligible effect on the Mechanical Work and Potential Energy hypotheses, decreased the amplitude of the Movement Torque hypothesis from 22° (factor 0.5) to 15° (factor 2), and increased the amplitude of the Postural Torque and Simplifying Strategy hypotheses from 22° and 5° (factor 0.5) to 26° and 13° (factor 2), respectively.

Acknowledgements

None.

Grants

None.

Disclosures

None.

References

Alexander RM. A minimum energy cost hypothesis for human arm trajectories. *Biological Cybernetics* 76: 97-105, 1997.

Anderton W, and Charles S. Kinematic coupling of wrist and forearm movements. In: *Annual Meeting of the American Society of Biomechanics*. Gainesville, FL: 2012.

Bernstein N. *The Co-ordination and Regulation of Movements*. Oxford, England: Pergamon Press Ltd., 1967.

Berret B, Chiovetto E, Nori F, and Pozzo T. Evidence for Composite Cost Functions in Arm Movement Planning: An Inverse Optimal Control Approach. *Plos Computational Biology* 7: 2011.

Burdet E, Franklin DW, and Milner TE. *Human Robotics*. Cambridge, MA: The MIT Press, 2013.

Campolo D, Accoto D, Formica D, and Guglielmelli E. Intrinsic Constraints of Neural Origin: Assessment and Application to Rehabilitation Robotics. *Ieee T Robot* 25: 492-501, 2009.

Campolo D, Formica D, Guglielmelli E, and Keller F. Kinematic analysis of the human wrist during pointing tasks. *Exp Brain Res* 201: 561-573, 2010.

Campolo D, Widjaja F, Esmaeili M, and Burdet E. Pointing with the wrist: a postural model for Donders' law. *Exp Brain Res* 212: 417-427, 2011.

Ceylan M, Henriques DYP, Tweed DB, and Crawford JD. Task-dependent constraints in motor control: Pinhole goggles make the head move like an eye. *J Neurosci* 20: 2719-2730, 2000.

Charles SK, and Hogan N. Dynamics of wrist rotations. *J Biomech* 44: 614-621, 2011.

Charles SK, and Hogan N. Stiffness, not inertial coupling, determines path curvature of wrist motions. *J Neurophysiol* 107: 1230-1240, 2012.

Craig JJ. *Introduction to Robotics*. Upper Saddle River, NJ: Pearson Prentice Hall, 2005.

Crawford JD, Martinez-Trujillo JC, and Klier EM. Neural control of three-dimensional eye and head movements. *Curr Opin Neurobiol* 13: 655-662, 2003.

Dolan JM, Friedman MB, and Nagurka ML. Dynamic and Loaded Impedance Components in the Maintenance of Human Arm Posture. *Ieee Transactions on Systems Man and Cybernetics* 23: 698-709, 1993.

Dounskaia N. The internal model and the leading joint hypothesis: implications for control of multi-joint movements. *Exp Brain Res* 166: 1-16, 2005.

Drake WB, and Charles SK. Passive Stiffness of Coupled Wrist and Forearm Rotations. *Annals of Biomedical Engineering* 42: 1853-1866, 2014.

Fitts PM. The information capacity of the human motor system in controlling the amplitude of movement. *J Exp Psychol* 47: 381-391, 1954.

Flash T, and Hogan N. The Coordination of Arm Movements - an Experimentally Confirmed Mathematical-Model. *J Neurosci* 5: 1688-1703, 1985.

Flash T, Meirovitch Y, and Barliya A. Models of human movement: Trajectory planning and inverse kinematics studies. *Robotics and Autonomous Systems* 61: 330-339, 2013.

Formica D, Charles SK, Zollo L, Guglielmelli E, Hogan N, and Krebs HI. The Passive Stiffness of the Wrist and Forearm. *J Neurophysiol* 108: 1158-1166, 2012.

Ganesh G, Haruno M, Kawato M, and Burdet E. Motor Memory and Local Minimization of Error and Effort, Not Global Optimization, Determine Motor Behavior. *J Neurophysiol* 104: 382-390, 2010.

Ghasia FF, and Angelaki DE. Do motoneurons encode the noncommutativity of ocular rotations? *Neuron* 47: 281-293, 2005.

Ghosh BK, and Wijayasinghe IB. Dynamics of Human Head and Eye Rotations Under Donders' Constraint. *Ieee Transactions on Automatic Control* 57: 2478-2489, 2012.

Gielen C, Vrijenhoek EJ, Flash T, and Neggers SFW. Arm position constraints during pointing and reaching in 3-D space. *J Neurophysiol* 78: 660-673, 1997.

Glenn B, and Vilis T. Violations of listings law after large eye and head gaze shifts. *J Neurophysiol* 68: 309-318, 1992.

Gomi H, and Osu R. Task-dependent viscoelasticity of human multijoint arm and its spatial characteristics for interaction with environments. *J Neurosci* 18: 8965-8978, 1998.

Halaki M, O'Dwyer N, and Cathers I. Systematic nonlinear relations between displacement amplitude and joint mechanics at the human wrist. *J Biomech* 39: 2171-2182, 2006.

Hore J, Watts S, and Tweed D. Arm position constraints when throwing in 3 dimensions. *J Neurophysiol* 72: 1171-1180, 1994.

Hore J, Watts S, and Vilis T. Constraints on arm position when pointing in 3 dimensions - donders law and the fick gimbal strategy. *J Neurophysiol* 68: 374-383, 1992.

Kunin M, Osaki Y, Cohen B, and Raphan T. Rotation axes of the head during positioning, head shaking, and locomotion. *J Neurophysiol* 98: 3095-3108, 2007.

Lacquaniti F, Terzuolo C, and Viviani P. The law relating the kinematic and figural aspects of drawing movements. *Acta Psychologica* 54: 115-130, 1983.

Latash ML. The bliss (not the problem) of motor abundance (not redundancy). *Exp Brain Res* 217: 1-5, 2012.

Liebermann DG, Biess A, Friedman J, Gielen C, and Flash T. Intrinsic joint kinematic planning. I: Reassessing the Listing's law constraint in the control of three-dimensional arm movements. *Exp Brain Res* 171: 139-154, 2006a.

Liebermann DG, Biess A, Gielen C, and Flash T. Intrinsic joint kinematic planning. II: Hand-path predictions based on a Listing's plane constraint. *Exp Brain Res* 171: 155-173, 2006b.

Loeb GE. Optimal isn't good enough. *Biological Cybernetics* 106: 757-765, 2012.

Marotta JJ, Medendorp WP, and Crawford JD. Kinematic rules for upper and lower arm contributions to grasp orientation. *J Neurophysiol* 90: 3816-3827, 2003.

Milner TE, and Cloutier C. Compensation for mechanically unstable loading in voluntary wrist movement. *Exp Brain Res* 94: 522-532, 1993.

Mohan V, and Morasso P. Passive motion paradigm: an alternative to optimal control. *Frontiers in neurorobotics* 5: 4, 2011.

Pando A, and Hernandez JC, SK. Wrist forces and torques during activities of daily living. In: *Annual Meeting of the Society for Neuroscience*. San Diego, CA: 2013.

Pando AL, Lee H, Drake WB, Hogan N, and Charles SK. Position-Dependent Characterization of Passive Wrist Stiffness. *Ieee T Bio-Med Eng* 61: 2235-2244, 2014.

Park K, Chang PH, and Kang SH. In Vivo Estimation of Human Forearm and Wrist Dynamic Properties. *Ieee T Neur Sys Reh* 25: 436-446, 2017.

Peaden AW, and Charles SK. Dynamics of wrist and forearm rotations. *J Biomech* 47: 2779-2785, 2014.

Perreault EJ, Kirsch RF, and Crago PE. Multijoint dynamics and postural stability of the human arm. *Exp Brain Res* 157: 507-517, 2004.

Radau P, Tweed D, and Vilis T. 3-dimensional eye, head, and chest orientations after large gaze shifts and the underlying neural strategies. *J Neurophysiol* 72: 2840-2852, 1994.

Salmond L, Davidson A, and Charles S. Proximal-distal differences in movement smoothness reflect differences in biomechanics. *J Neurophysiol* 117: 1239-1257, 2017.

Scholz JP, Schoner G, and Latash ML. Identifying the control structure of multijoint coordination during pistol shooting. *Exp Brain Res* 135: 382-404, 2000.

Seegmiller D, Eggett DL, and Charles SK. The effect of common wrist orthoses on the stiffness of wrist rotations. *J Rehabil Res Dev* 53: 1151-1166, 2016.

Simon HA. Rational choice and the structure of the environment. *Psychological Review* 63: 129-138, 1956.

Soechting JF, Buneo CA, Herrmann U, and Flanders M. Moving effortlessly in 3-dimensions - does donders-law apply to arm movement. *J Neurosci* 15: 6271-6280, 1995.

Solnik S, Pazin N, Coelho CJ, Rosenbaum DA, Scholz JP, Zatsiorsky VM, and Latash ML. End-state comfort and joint configuration variance during reaching. *Exp Brain Res* 225: 431-442, 2013.

Solnik S, Pazin N, Coelho CJ, Rosenbaum DA, Zatsiorsky VM, and Latash ML. Postural sway and perceived comfort in pointing tasks. *Neuroscience Letters* 569: 18-22, 2014.

Tagliamonte NL, Scorcia M, Formica D, Campolo D, and Guglielmelli E. Effects of Impedance Reduction of a Robot for Wrist Rehabilitation on Human Motor Strategies in Healthy Subjects during Pointing Tasks. *Adv Robotics* 25: 537-562, 2011.

Thurtell MJ, Joshi AC, and Walker MF. Three-dimensional kinematics of saccadic and pursuit eye movements in humans: Relationship between Donders' and Listing's laws. *Vision Research* 60: 7-15, 2012.

Tommasino P, and Campolo D. Task-space separation principle: a force-field approach to motion planning for redundant manipulators. *Bioinspiration & Biomimetics* 12: 2017.

Tsuji T, Morasso PG, Goto K, and Ito K. Human Hand Impedance Characteristics During Maintained Posture. *Biological Cybernetics* 72: 475-485, 1995.

Tweed D. Three-dimensional model of the human eye-head saccadic system. *J Neurophysiol* 77: 654-666, 1997.

Viviani P, and Schneider R. A developmental-study of the relationship between geometry and kinematics in drawing movements. *Journal of Experimental Psychology-Human Perception and Performance* 17: 198-218, 1991.

Wu G, van der Helm FCT, Veeger HEJ, Makhsous M, Van Roy P, Anglin C, Nagels J, Karduna AR, McQuade K, Wang XG, Werner FW, and Buchholz B. ISB recommendation on definitions of joint coordinate systems of various joints for the

reporting of human joint motion - Part II: shoulder, elbow, wrist and hand. *J Biomech* 38: 981-992, 2005.
Yang JF, and Scholz JP. Learning a throwing task is associated with differential changes in the use of motor abundance. *Exp Brain Res* 163: 137-158, 2005.

Tables

Table 1: Data fit for the movements of Experiment 1 (small-slow only): Amplitude, frequency, phase, and correlation coefficient R of the sinusoidal fit of the PS-angle $\Delta \boldsymbol{p}$ vs. target angle $\boldsymbol{\theta}$ for each subject's movements in Figure 6A. Subjects 9, 14, and 20 had values fit parameters (indicated by asterisks) beyond 2 SD from the mean and were excluded from the analysis.

Subject	**Amplitude [deg]**	**Frequency [cycles/rev]**	**Phase [deg]**	**R**
1	1.82	1.04	121	0.79
2	2.10	1.12	184	0.89
3	1.74	0.90	102	0.78
4	1.92	1.06	149	0.93
5	2.19	1.07	188	0.94
6	0.71	1.09	182	0.70
7	0.47	1.19	174	0.38
8	1.77	1.06	103	0.86
9	3.61*	0.96	112	0.41
10	1.15	1.04	132	0.85
11	1.35	0.96	166	0.78
12	1.26	1.05	169	0.73
13	0.95	0.99	125	0.76
14	1.40	1.14	44*	0.74
15	1.33	1.02	148	0.82
16	1.56	1.03	115	0.75
17	1.12	1.04	140	0.87
18	1.10	0.98	163	0.85
19	1.35	1.14	114	0.81
20	1.43	0.85*	139	0.76
Mean	**1.52**	**1.04**	**138**	**0.77**
SD	**0.66**	**0.08**	**36**	**0.14**

Table 2: Effect of distance and speed on the amplitude, frequency, phase, and fit of PS-angle $\Delta\boldsymbol{p}$.

Dependent Variable	**Independent Variable**	**F-Value**	**p-Value**
Amplitude	Distance	24.88	**0.0001**
	Speed	3.38	0.103
	Distance*Speed	0.29	0.612
Frequency	Distance	13.92	**0.002**
	Speed	6.59	**0.033**
	Distance*Speed	7.61	**0.040**
Phase	Distance	0.48	0.497
	Speed	5.63	**0.045**
	Distance*Speed	0.44	0.537
R	Distance	1.64	0.219
	Speed	1.04	0.337
	Distance*Speed	0.02	0.896

Table 3: Data fit for the movements of Experiment 2: Amplitude, frequency, phase, and correlation coefficient R of the sinusoidal fit of the PS-angle $\Delta\boldsymbol{p}$ vs. target angle $\boldsymbol{\theta}$ for each subject's movements in Figure 6B. Subject 30 had one fit parameter (indicated by asterisk) beyond 2 SD from the mean and was excluded from the analysis.

Subject	**Amplitude [deg]**	**Frequency [cycles/rev]**	**Phase [deg]**	**R**
21	2.53	1.02	145	0.72
22	1.76	1.00	171	0.82
23	1.51	1.04	127	0.73
24	1.58	1.01	119	0.78
25	1.62	0.97	182	0.90
26	2.22	1.04	165	0.70
27	2.38	1.05	112	0.81
28	1.65	1.04	121	0.71
29	4.07	1.08	124	0.62
30	5.13*	1.10	95	0.78
Mean	**2.45**	**1.04**	**136**	**0.76**
SD	**1.22**	**0.04**	**28**	**0.08**

Table 4: Effect of constraining PS at the center target (Experiment 2 vs. Experiment 1) on the amplitude, frequency, phase, and fit of PS-angle $\Delta\boldsymbol{p}$.

Dependent Variable	**F-Value**	**p-Value**
Amplitude	8.70	**0.007**
Frequency	0.47	0.502
Phase	0.17	0.680
R	0.71	0.408

Figures

Figure 1: Experimental setup. A: Subjects were required to rotate their wrist and forearm in combinations of wrist flexion-extension (FE), wrist radial-ulnar deviation (RUD), and forearm pronation-supination (PS) to move a cursor (dark gray circle) toward one of 16 peripheral targets (light gray circles) on a screen. The coordinates of the cursor on the screen are given by $\boldsymbol{x_s}$ and $\boldsymbol{y_s}$. PS occurs about the body-fixed $\boldsymbol{y_w}$-axis (dashed because it passes through the forearm and is not visible from the outside) and is indicated by $\boldsymbol{p}$ (pronation is positive), FE occurs about the body-fixed $\boldsymbol{z_w}$-axis and is indicated by $\boldsymbol{f}$(flexion is positive), and RUD occurs about the body-fixed $\boldsymbol{x_w}$-axis and is indicated by $\boldsymbol{u}$ (ulnar deviation is positive). When the wrist and forearm are in neutral position (shown), the cursor representing the pointing direction is in the center target. B-C: Pointing toward a peripheral target can be accomplished through infinitely many combinations of PS, FE, and RUD, including without PS (B) or with PS (C). Rotating in PS rotates the rotation axes of FE and RUD ($\boldsymbol{z_w}$ and $\boldsymbol{x_w}$, respectively), as shown in C.

Figure 2: Methodology for computing the predicted output of the simplifying strategy hypothesis. Movements to a new target (given by $\boldsymbol{x_s}, \boldsymbol{y_s}$) were planned using only FE and RUD ($\boldsymbol{f}, \boldsymbol{u}$), but executed in a forearm and wrist system that included all PS as well as FE and RUD), resulting in joint displacements ($\boldsymbol{p}', \boldsymbol{f}', \boldsymbol{u}'$). The change in PS ($\boldsymbol{\Delta p}$) was calculated from $\boldsymbol{p}'$.

Figure 3: Example of movement over time, and how final measures were defined. A: One subject's pronation-supination angle $\boldsymbol{p}$ (positive in pronation) as a function of time for an entire session. In addition to changes in $\boldsymbol{p}$ that occurred for individual movements (visible as little spikes), subjects generally showed a drift in $\boldsymbol{p}$ over the duration of the session. B: Close-up view of an 8-second portion of the plot in A that shows movement-by-movement changes in $\boldsymbol{p}$. Each dashed vertical line indicates when a new target appeared (prompting the user to move), and the following solid vertical line indicates when the subject entered that target. C: Same as B, but with graphs representing FE angle $\boldsymbol{f}$ (positive in flexion) and RUD angle $\boldsymbol{u}$ (positive in ulnar deviation) to demonstrate that changes in $\boldsymbol{p}$ were relatively small. D: The change in $\boldsymbol{p}$ that occurred during a movement ($\Delta\boldsymbol{p}$) was calculated as the difference between $\boldsymbol{p}$ at the beginning and ending of the movement ($\boldsymbol{p_i}$ and $\boldsymbol{p_f}$, respectively). The target angle $\boldsymbol{\theta}$ was expressed in terms of the wrist coordinate frame at the time the target appeared, i.e. $\boldsymbol{\theta} = \boldsymbol{\phi} + \boldsymbol{p_i}$, where $\boldsymbol{\phi}$ is the angle of the target expressed in the screen coordinate frame ($\boldsymbol{x_s}, \boldsymbol{y_s}$), and the initial wrist coordinate frame is represented by the intial FE and RUD rotation axes $\boldsymbol{z_{w,init}}$ and $\boldsymbol{x_{w,init}}$, respectively.

Figure 4: The hypothesized control strategies predicted similar behavior in FE-angle $\boldsymbol{f}$ (A) and similar behavior in RUD-angle $\boldsymbol{u}$ (B), but significantly different behavior in PS-angle $\boldsymbol{p}$ (C). The control strategies include minimization of mechanical work (MW), movement torque (MT), postural torque (PT), potential energy (PE), path length (PL), as well as the simplifying strategy (SS).

Figure 5: FE-angle $\boldsymbol{f}$, RUD-angle $\boldsymbol{u}$, and PS-angle $\Delta\boldsymbol{p}$ vs. target angle $\boldsymbol{\theta}$ for all subjects in experiment 1 (A; small-slow only) and experiment 2 (B). Angles $\boldsymbol{f}$, $\boldsymbol{u}$, and $\Delta\boldsymbol{p}$ are marked by black dots, dark gray x's, and light gray, solid circles, respectively, and are positive in flexion, ulnar deviation, and pronation. The number in each box is the same subject identifier used in

Table 1 and Table 3. Target angles ($\boldsymbol{\theta}$) of 0°, 90°, 180°, and 270° correspond to targets in pure radial deviation, extension, ulnar deviation, and flexion, respectively.

Figure 6: PS-angle $\Delta\boldsymbol{p}$ vs. target angle $\boldsymbol{\theta}$ for all subjects in experiment 1 (A: small-slow only) and experiment 2 (B), together with sinusoidal fits. Angle $\Delta\boldsymbol{p}$ is positive in pronation. The number in each box is the same subject identifier used in Table 1 and Table 3. Target angles ($\boldsymbol{\theta}$) of 0°, 90°, 180°, and 270° correspond to targets in pure radial deviation, extension, ulnar deviation, and flexion, respectively.

Figure 7: Sinusoidal fits of PS-angle $\Delta\boldsymbol{p}$ vs. target angle $\boldsymbol{\theta}$ for all subjects in Experiment 1 (A; small-slow only) and Experiment 2 (B). Each subject's sinusoidal fit is shown as a thin gray line, and the mean across all subjects is shown as the thick black line. Target angles $\boldsymbol{\theta}$ of 0°, 90°, 180°, and 270° correspond to targets in pure radial deviation, extension, ulnar deviation, and flexion, respectively.

Figure 8: Simulated PS-angle $\Delta\boldsymbol{p}$ vs. target angle $\boldsymbol{\theta}$ for each hypothesized control strategy, compared to the experimentally observed PS angle (thick black curve). A: Initial set of simulations using passive stiffness. None of the control strategies match the experiment well. The Simplifying Strategy (SS) hypothesis matches the experiment in shape (sinusoid) and frequency (1 cycle in $\Delta\boldsymbol{p}$ per revolution in $\boldsymbol{\theta}$), but its amplitude is too large. The Path Length (PL) hypothesis matches the experiment in amplitude and shape (sinusoid) but not in frequency (2 cycles/rev). The Mechanical Work (MW), Potential Energy (PE), Movement Torque (MT), and Postural Torque (PT) hypotheses differ from the experimentally observed pattern in multiple aspects. B: Increasing the model stiffness within a physiologically plausible range caused three hypotheses to approach the experiment. This was true for: the Simplifying Strategy hypothesis if $\boldsymbol{K_{pp}}$was increased ($\uparrow \boldsymbol{K_{pp}}$) or if $\boldsymbol{K_{pp}}$ and $\boldsymbol{K}$ were increased ($\uparrow \boldsymbol{K_{pp}}\&\boldsymbol{K}$); the Movement Torque hypothesis if $\boldsymbol{K_{pp}}$was increased; and the Postural Torque hypothesis if $\boldsymbol{K_{pp}}$was increased or if $\boldsymbol{K_{pp}}$ and $\boldsymbol{K}$ were increased. The Simplifying Strategy fit the best and the most robustly. Note that the mean of the experimental data was ignored before applying the sinusoidal fit, so the difference in absolute values between the hypotheses and the experiment should be ignored.

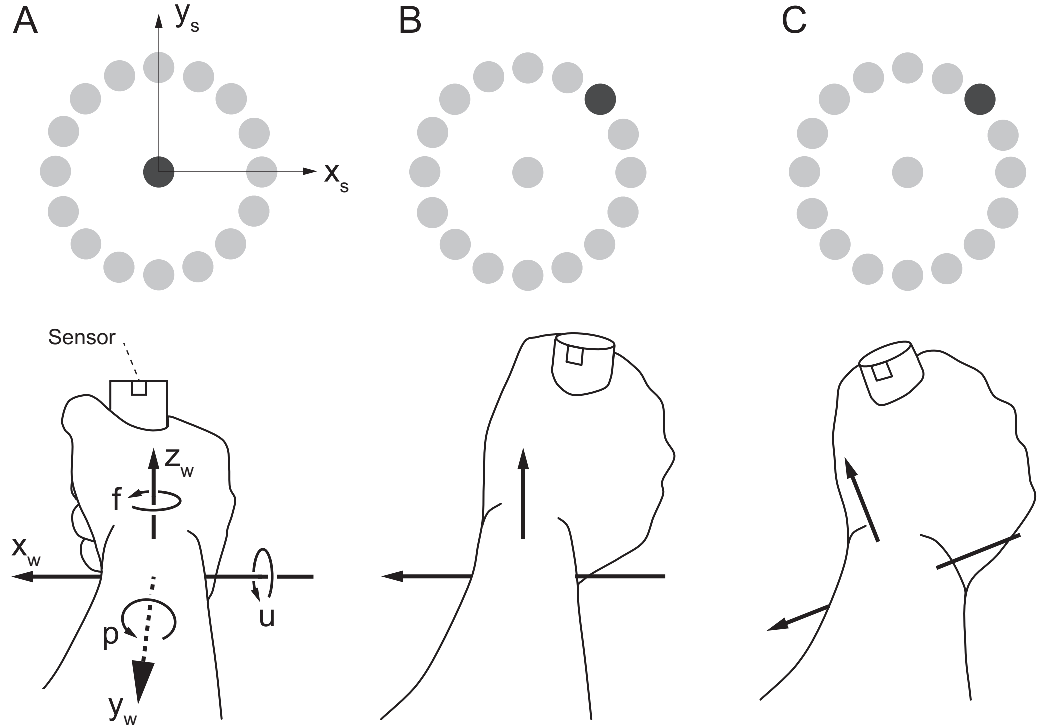
A
B
C
y_s
x_s
Sensor
z_w
f
x_w
u
p
y_w

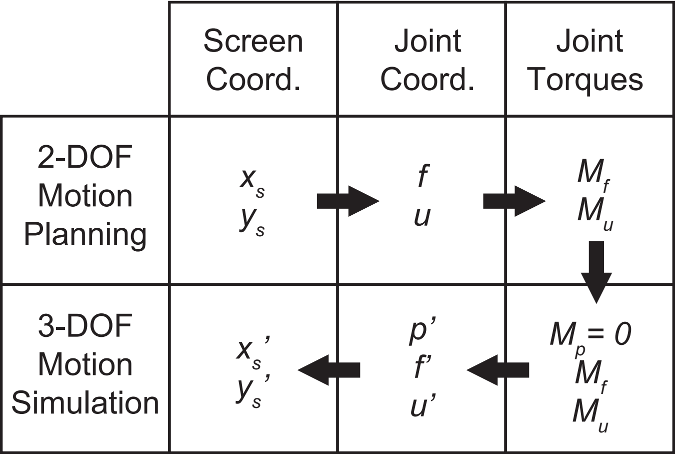
Screen Coord.
Joint Coord.
Joint Torques
2-DOF Motion Planning
3-DOF Motion Simulation
x_s
y_s
f
u
M_f
M_u
$M_p = 0$
M_f
M_u
p'
f'
u'
x_s',
y_s'

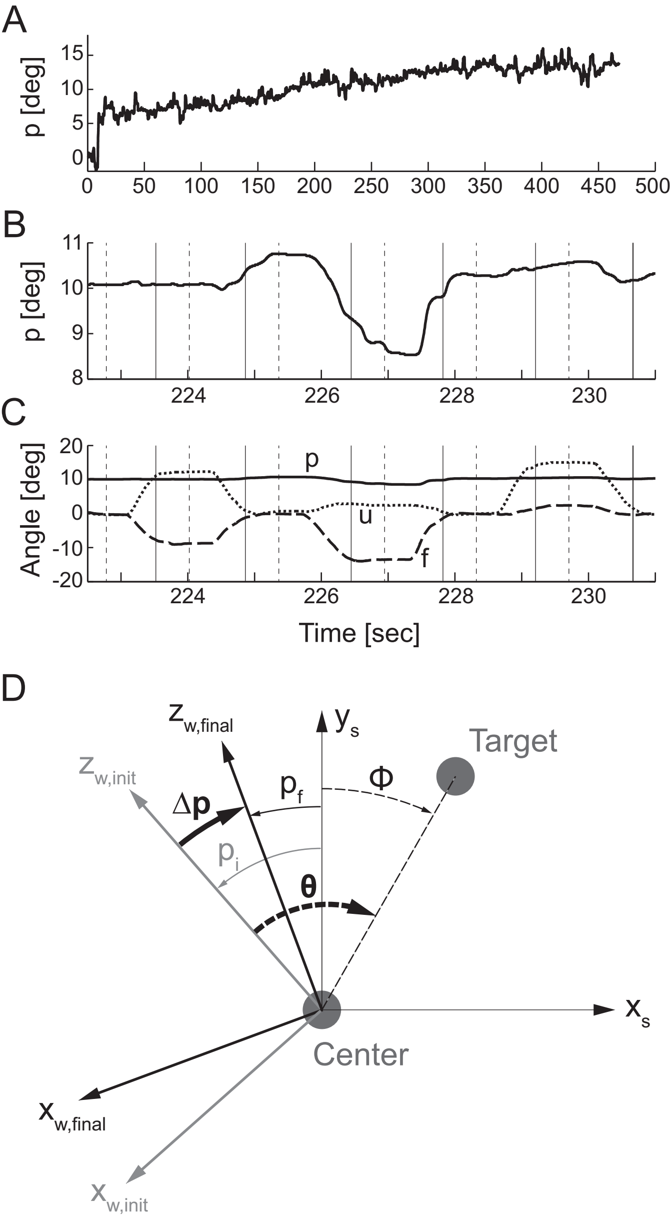
A
p [deg]
15
10
5
0
0
50
100
150
200
250
300
350
400
450
500
B
p [deg]
11
10
9
8
224
226
228
230
C
Angle [deg]
20
10
0
-10
-20
p
u
f
224
226
228
230
Time [sec]
D
$z_{w,final}$
y_s
Target
$z_{w,init}$
Φ
p_f
Δ**p**
p_i
θ
x_s
Center
$x_{w,final}$
$x_{w,init}$

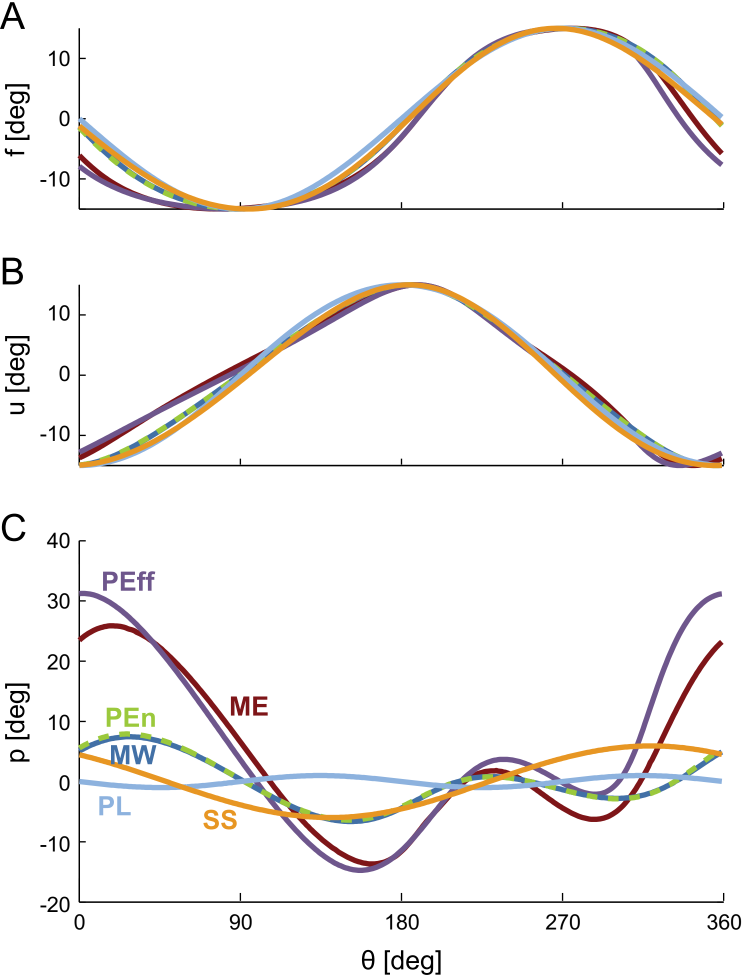
A
B
C
f [deg]
u [deg]
p [deg]
10
0
-10
40
30
20
-20
PEff
ME
PEn
MW
PL
SS
0
90
180
270
360
θ [deg]

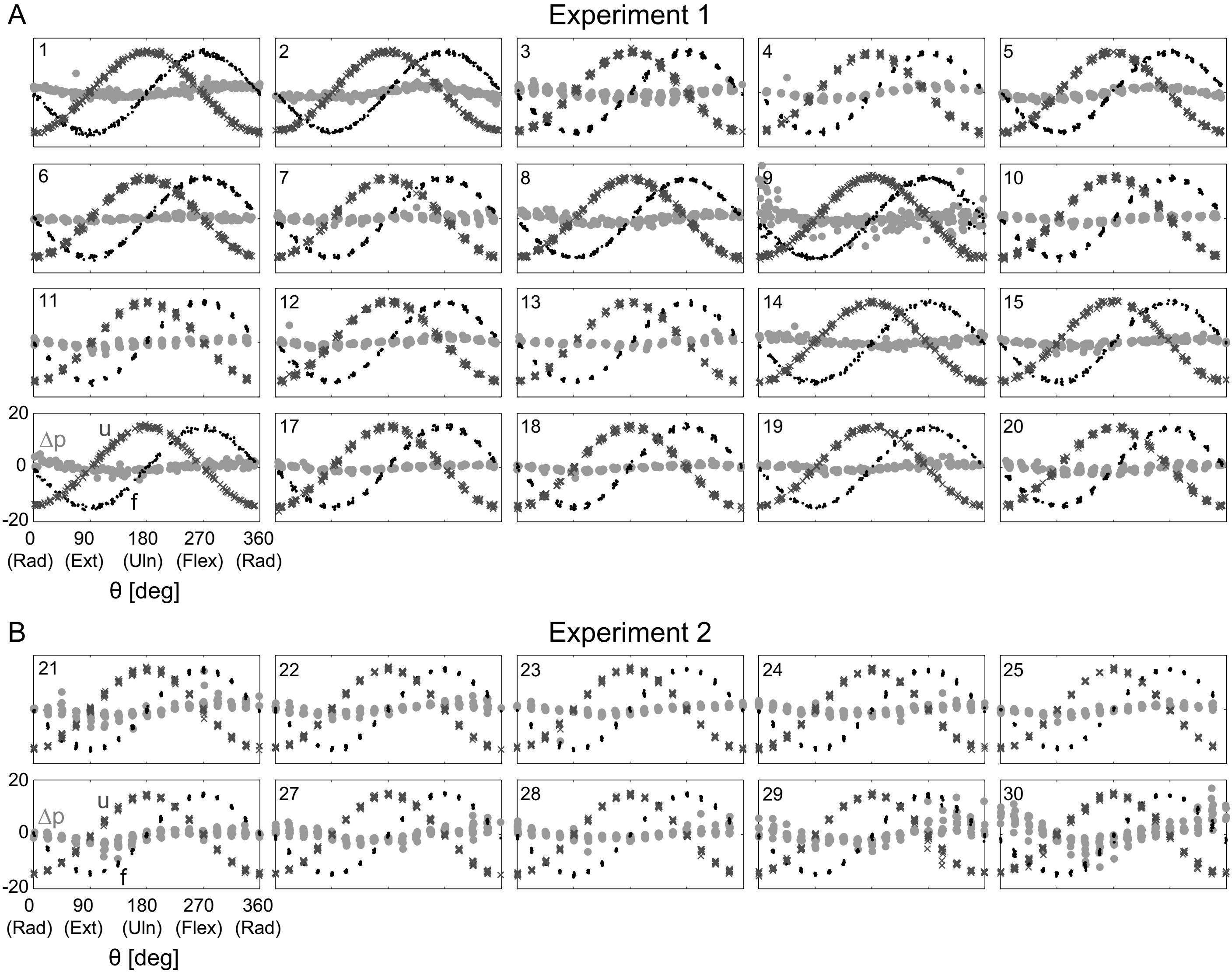
A
Experiment 1
1
2
3
4
5
6
7
8
9
10
11
12
13
14
15
16
17
18
19
20
f, u, Δp [deg]
Δp
u
f
20
0
-20
0
90
180
270
360
(Rad)
(Ext)
(Uln)
(Flex)
(Rad)
θ [deg]
B
Experiment 2
21
22
23
24
25
26
27
28
29
30
f, u, Δp [deg]
Δp
u
f
20
0
-20
0
90
180
270
360
(Rad)
(Ext)
(Uln)
(Flex)
(Rad)
θ [deg]

A

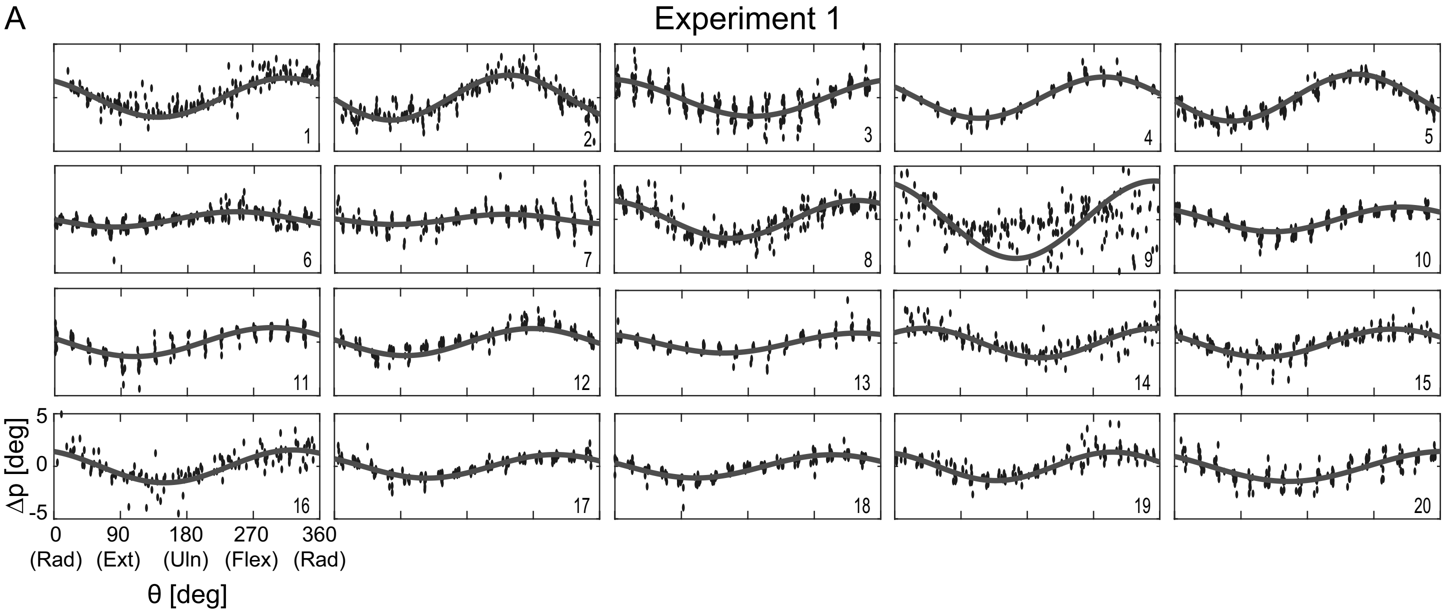
Experiment 1
Δp [deg]
θ [deg]
0 (Rad) 90 (Ext) 180 (Uln) 270 (Flex) 360 (Rad)
5
0
-5
1 2 3 4 5 6 7 8 9 10 11 12 13 14 15 16 17 18 19 20

B

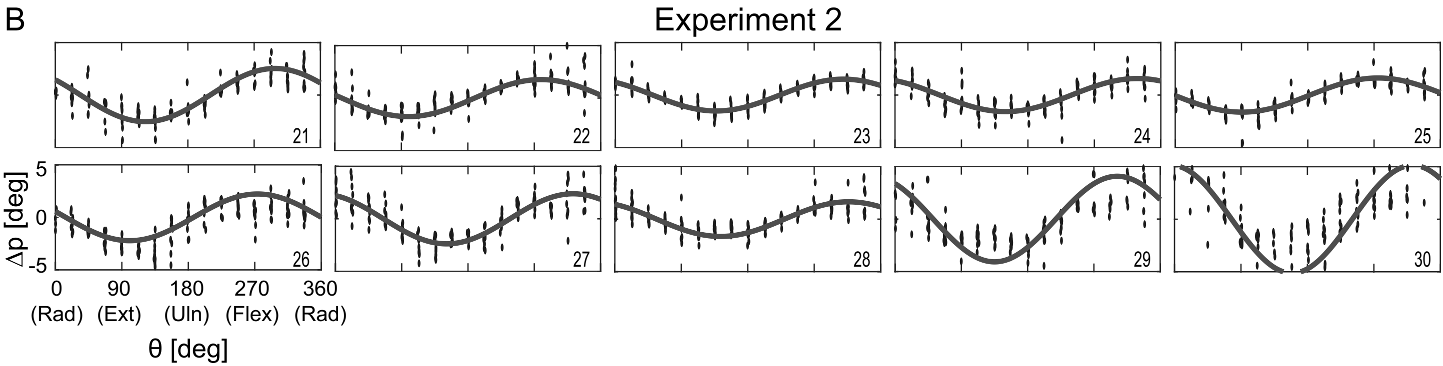
Experiment 2
Δp [deg]
θ [deg]
0 (Rad) 90 (Ext) 180 (Uln) 270 (Flex) 360 (Rad)
5
0
-5
21 22 23 24 25 26 27 28 29 30

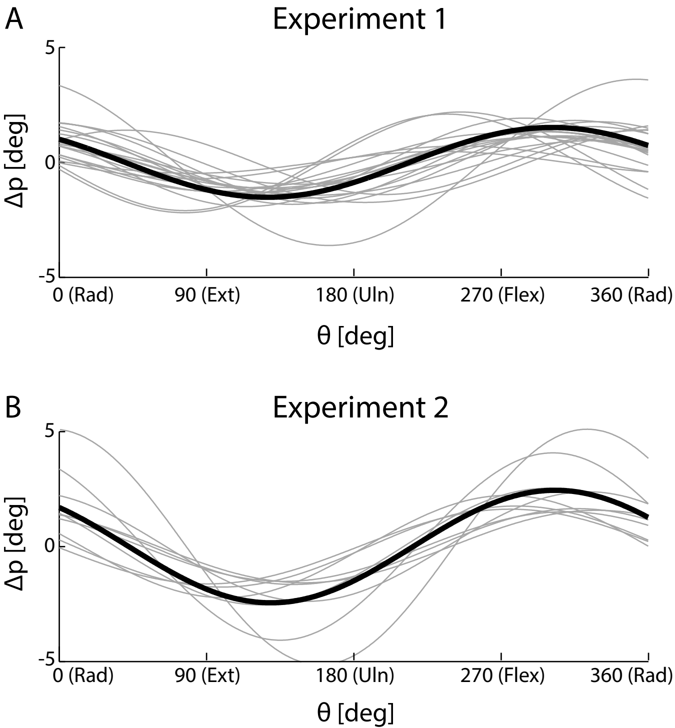
A
Experiment 1
5
0
-5
Δp [deg]
0 (Rad)
90 (Ext)
180 (Uln)
270 (Flex)
360 (Rad)
θ [deg]
B
Experiment 2
5
0
-5
Δp [deg]
0 (Rad)
90 (Ext)
180 (Uln)
270 (Flex)
360 (Rad)
θ [deg]

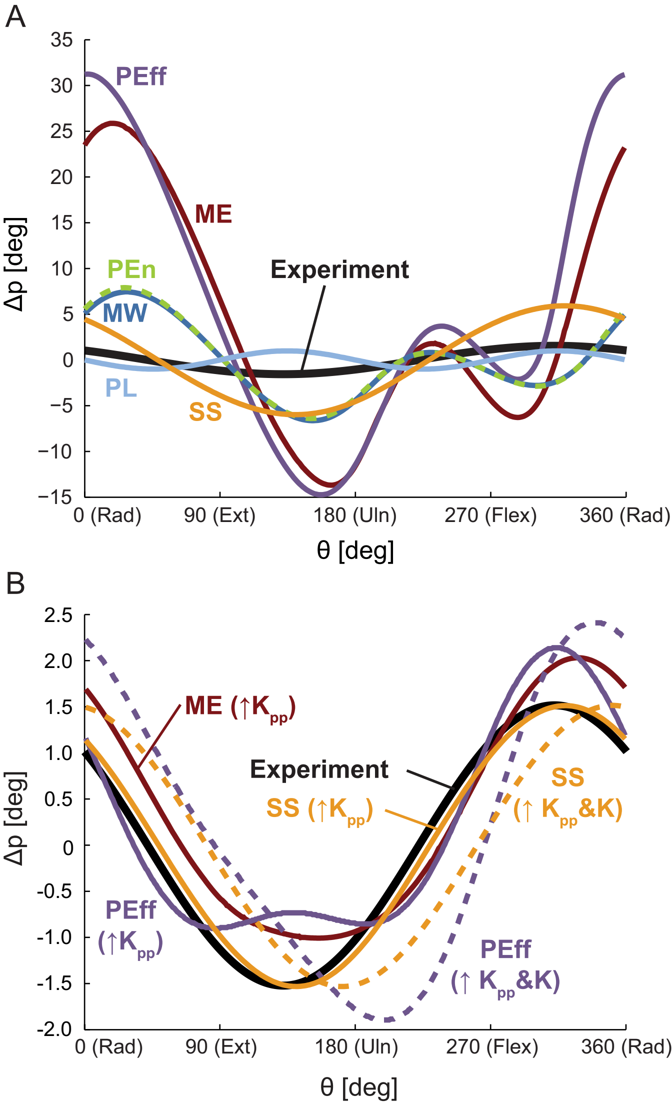
A
35
30
25
20
15
10
5
0
−5
−10
−15
Δp [deg]
PEff
ME
PEn
MW
Experiment
PL
SS
0 (Rad)
90 (Ext)
180 (Uln)
270 (Flex)
360 (Rad)
θ [deg]
B
2.5
2.0
1.5
1.0
0.5
0
-0.5
-1.0
-1.5
-2.0
Δp [deg]
ME (↑K_pp)
Experiment
SS (↑K_pp)
SS (↑ K_pp&K)
PEff (↑K_pp)
PEff (↑ K_pp&K)
0 (Rad)
90 (Ext)
180 (Uln)
270 (Flex)
360 (Rad)
θ [deg]